arXiv:0911.3453v2 [hep-lat] 10 Jun 2010

Effective Potential in the Strong-coupling Lattice QCD with Next-to-Next-to-Leading Order Effects

Takashi Z. Nakano[1], Kohtaroh Miura[2] and Akira Ohnishi[2]

[1]*Department of Physics, Kyoto University, Kyoto 606-8502, Japan*
[2]*Yukawa Institute for Theoretical Physics, Kyoto University, Kyoto 606-8502, Japan*

We derive an analytic expression of the effective potential at finite temperature (T) and chemical potential (μ) in the strong-coupling lattice QCD for color $SU(3)$ including next-to-next-to-leading order (NNLO) effects in the strong coupling expansion. NNLO effective action terms are systematically evaluated in the leading order of the large dimensional ($1/d$) expansion, and are found to come from some types of connected two plaquette configurations. We apply the extended Hubbard-Stratonovich transformation and a gluonic dressed fermion technique to the effective action, and obtain the effective potential as a function of T, μ, and two order parameters; chiral condensate and a vector potential field. The next-to-leading order (NLO) and NNLO effects result in modifications of the wave function renormalization factor, quark mass and chemical potential. We find that $T_{c,\mu=0}$ and $\mu_{c,T=0}$ are similar to the NLO results, whereas the position of the critical point is sensitive to NNLO corrections.

§1. Introduction

Understanding the Quantum Chromodynamics (QCD) phase diagram is one of the most interesting problems in quark and hadron physics. In the present Relativistic Heavy-Ion Collider (RHIC) experiments, phase transition to strongly coupled matter consisting of quarks and gluons seems to be observed.1) The QCD phase transition observed at RHIC takes place at almost zero baryon density, where the predictions of lattice QCD Monte-Carlo (MC) simulations are reliable. The phase transition of compressed baryonic matter will be probed in the future experiments in FAIR, J-PARC and low energy programs at RHIC. At finite baryon densities, the lattice MC simulations are difficult due to the complex fermion determinant.2) In order to discuss the whole shape of the phase diagram, it is necessary to invoke some approximations in QCD or to apply effective models. The strong-coupling lattice QCD (SC-LQCD) is one of the most instructive approximations to investigate the phase structure at finite temperature T and chemical potential μ.

SC-LQCD was first applied to the pure Yang-Mills theory. Wilson showed that the Wilson loop would follow the area law at strong coupling,3) and the Creutz demonstrated that the lattice MC simulation can connect strong coupling and weak coupling (perturbative) expressions of the string tension.4) The behavior of the string tension as a function of the inverse coupling, $\beta = 2N_c/g^2$, is well understood in the strong coupling and character expansions, which were developed by Münster.5) Chiral symmetry in SC-LQCD also has been long studied from 1980s. Basic formulations has been developed based on the staggered,6),7) Wilson6),8) and naïve9) fermions. The domain-wall10) and the overlap11) fermion provide modern formulation of the lattice chiral symmetry, and some SC-LQCD based investigations are found in Refs. 12), 13) (domain-wall) and 14), 15) (overlap). In the strong coupling limit (SCL), chiral symmetry is spontaneously broken in vacuum,6)–9), 12)–14) and restored at high T and/or large μ.15)–28)

Since the SC-LQCD is based on the same formulation as the lattice MC simulations, its results should be consistent with the MC results such as hadron mass spectrum29)–31) as long as the applied approximations are valid. The phase diagram structure has been predicted in the strong coupling limit,16), 22)–25), 27) and it is recently confirmed qualitatively in MC simulations32) based on the monomer-dimer-polymer (MDP) formalism.33) In order to make a step forward towards the true phase diagram, it is necessary to develop the formalism to include the plaquette effects both in lattice MC simulations at finite μ and SC-LQCD. There exists some SC-LQCD works including NLO effects, *i.e.* one plaquette contributions, on the hadron masses29)–31) and the phase diagram.21), 34), 35) In our previous work on the NLO SC-LQCD,34) we find that the phase diagram evolves to an empirical shape with increasing $\beta = 6/g^2$, while the critical temperature at zero chemical potential $T_{c,\mu=0}$ is larger than the MC results. The later observation suggests that we need to evaluate the next-to-next-to-leading order (NNLO) effects on the phase diagram, which have never been investigated before.

In this paper, we derive an analytic expression of the effective potential including NNLO effects at finite T and μ, and investigate NNLO contributions to the phase diagram. We adopt one species of unrooted staggered fermion corresponding to $N_f = 4$ in the continuum region. Since the flavor dependence of the phase boundary has been shown to be moderate,22), 25), 36) the present results could be valuable for the understanding of the phase diagram with $N_f = 2 + 1$. Effective action terms from one and two plaquette configurations are obtained by integrating out spatial link variables. We apply the extended Hubbard-Stratonovich transformation34), 35) to bosonize fermion interaction terms. With the $1/g^4$ corrections, we encounter those terms containing the next-to-nearest neighbor (NNN) interaction, which can be evaluated by introducing a gluonic dressed fermion. The effective potential is obtained as a function of T, μ and two order parameters: the chiral condensate and the quark number density. We determine the equilibrium from the stationary condition of the effective potential with respect to the auxiliary fields, and study the properties of QCD phase diagram. MC studies based on one species of unrooted staggered fermions have been carried out extensively around $\beta \sim 5$.36)–40) For the comparison between SC-LQCD results and those in the MC simulations, we discuss the results in the region $\beta \leq 6$. As shown later, the comparison of NNLO and NLO results suggests that β values under consideration are in conversion radius. We compare the critical temperature at $\mu = 0$ ($T_{c,\mu=0}$) with the NLO and MC results. We also study the evolution of the phase diagram and the critical point, as well as the possibility to have partially chiral restored matter, which has been suggested in NLO SC-LQCD.34), 35)

The QCD phase transition has another aspect of the deconfinement transition. In order to discuss the deconfinement transition, it is necessary to include the Polyakov loop effects as discussed in the framework of SC-LQCD19), 20), 28) and in the Nambu-Jona-Lasinio model with the Polyakov loop (PNJL) .53), 54) In this study, we concentrate on the chiral phase transition, and the simultaneous description of chiral and deconfinement transitions will be reported elsewhere.45)

On the phase transition study with unrooted staggered fermion, we still have some debate. In the strong coupling limit, the effective action with one species of unrooted staggered fermion is in the same universality class as the three-dimensional $O(2)$ spin models, and the phase transition is the second order .52) In the continuum region, one species of unrooted staggered fermion corresponds to four flavors (or tastes). The phase transition at $\mu = 0$ is expected to be the first order for $N_f \geq 3$ from the anomaly argument.47) The axial anomaly may cancel from the doublers on the lattice,50) but it is discussed that the conventional staggered anomaly appears in the taste-singlet PCAC relation.48) In numerical MC simulations,36) the transition at $\mu = 0$ is shown to be the first order in the continuum region. While we have these complications, the staggered fermions has a merit that it is simple. As a result, it is fast in numerical simulations, and it is possible to carry out the analytic calculations in the mean field approximations when we adopt the unrooted staggered fermion.

This paper is organized as follows. In §2, we derive the effective potential with $1/g^4$ corrections. In §3, we show the calculated results of the effective potential and the phase structure. We summarize our work in §4. All through this paper, we use the lattice unit $a = 1$, and physical values are shown in dimensionless values normalized by the lattice spacing a.

§2. Effective Potential in NNLO SC-LQCD

In this section, we derive the effective potential in SC-LQCD with NNLO corrections ($1/g^4$) at finite temperature T and chemical potential μ. We start from the lattice QCD action with one species of unrooted staggered fermion ($n_f = 1$) for color $SU(N_c)$ (§ 2.1), which corresponds to $N_f = 4n_f = 4$ in the continuum limit. After a short review on SCL and NLO effective action (§ 2.2), we derive the NNLO effective action (§ 2.3). Interaction terms are reduced into a bilinear form of fermions through the extended Hubbard-Stratonovich transformation (§ 2.4) and by introducing a gluonic dressed fermion (§ 2.5). We obtain an analytic expression of the effective potential in § 2.6.

2.1. *Lattice QCD action*

The lattice QCD action and the partition function with one species of staggered fermion for color $SU(N_c)$ are given as follows

$$\mathcal{Z}_{\rm LQCD} = \int \mathcal{D}[\chi,\bar{\chi},U_\nu]\ e^{-S_{\rm LQCD}} = \int \mathcal{D}[\chi,\bar{\chi},U_\nu]\ e^{-S_F^{(\tau)}-S_F^{(s)}-S_G}\ , \tag{2·1}$$

$$S_F^{(\tau)} = \frac{1}{2}\sum_x (V_x^+ - V_x^-) + m_0 \sum_x M_x\ , \tag{2·2}$$

$$S_F^{(s)} = \frac{1}{2}\sum_x \sum_{j=1}^{d} \eta_{j,x}\left[\bar{\chi}_x U_{j,x}\chi_{x+\hat{j}} - \bar{\chi}_{x+\hat{j}} U_{j,x}^\dagger \chi_x\right]\ , \tag{2·3}$$

$$S_G = -\frac{1}{g^2}\sum_x\sum_{j>0}\left[\mathrm{tr}\,U_{0j,x} + \mathrm{tr}\,U^\dagger_{0j,x}\right] - \frac{1}{g^2}\sum_x\sum_{k>j>0}\left[\mathrm{tr}\,U_{jk,x} + \mathrm{tr}\,U^\dagger_{jk,x}\right] \ , \qquad (2\cdot4)$$

where $\chi(\bar{\chi})$, m_0, $U_{0,x}(U_{j,x})$, and $U_{0j,x}$ $(U_{jk,x})$ denote the quark (anti-quark) field, the bare quark mass, temporal (spatial) link variable, and temporal (spatial) plaquette, respectively. The spinor structure is compressed into the staggered phase factor $\eta_{j,x} = (-1)^{x_0+\cdots+x_{j-1}}$.[6),41),42)] We have introduced two types of mesonic composites

$$V^+_x = \bar{\chi}_x e^{\mu} U_{0,x}\chi_{x+\hat{0}} \ , \quad V^-_x = \bar{\chi}_{x+\hat{0}} e^{-\mu} U^\dagger_{0,x}\chi_x \ , \quad M_x = \bar{\chi}_x\chi_x \ , \qquad (2\cdot5)$$

which appear in the effective action discussed later. Quark chemical potential μ on the lattice is introduced as a weight of the temporal hopping in $V^\pm$.[43)] By using a γ_5-related factor $\epsilon_x = (-1)^{x_0+\cdots+x_d}$, a staggered chiral transformation is given as $\chi_x \to e^{i\theta\epsilon_x}\chi_x$.[6),41),42)] The lattice kinetic action $S_F^{(\tau,s)}$ is invariant under this chiral transformation in the chiral limit $m_0 \to 0$. Throughout this paper, we consider the case of color $SU(N_c = 3)$ in 3+1 dimension $(d = 3)$ spacetime. Temporal and spatial lattice sizes are denoted as N_τ and L, respectively. While $T = 1/N_\tau$ takes discrete values, we consider T as a continuous valued temperature. We take account of finite T effects by imposing periodic and anti-periodic boundary conditions on link variables and quark fields, respectively. We take the static and diagonalized gauge (called Polyakov gauge) for temporal link variables with respect for the periodicity.[16)] In these setups, we evaluate the effective potential $\mathcal{F}_{\mathrm{eff}} = -\log\left[\mathcal{Z}_{\mathrm{LQCD}}\right]/(N_\tau L^d)$ based on the strong coupling expansion.

2.2. *Strong coupling expansion and SCL and NLO effective action*

In a finite T treatment of SC-LQCD, we first derive an effective action by integrating out the spatial links U_j, and the temporal link variable U_0 is evaluated later. The U_j integral can be exactly performed in each order of the $1/g^2$ expansion by utilizing the link integral formulae

$$\int dU\, U_{ab}\, U^\dagger_{cd} = \frac{1}{N_c}\delta_{ad}\,\delta_{bc} \ , \qquad \int dU\, U_{ab}\, U_{cd}\cdots U_{ef} = \frac{1}{N_c!}\varepsilon_{ac\cdots e}\,\varepsilon_{bd\cdots f} \ , \qquad (2\cdot6)$$

and so on. Then an isotropic hopping structure of hadronic composites emerges, and enables us to simplify the effective action by utilizing another expansion: $1/d$ expansion, which is explained in the next subsection.

In this work, we consider the effective action including the SCL $(1/g^0)$, NLO $(1/g^2)$ and NNLO $(1/g^4)$ terms in the strong coupling expansion, while we keep only the leading order terms $(1/d^0)$ in the $1/d$ expansion. The effective action is defined as

$$\begin{aligned} e^{-S_{\mathrm{eff}}(\chi,\bar{\chi},U_0)} &= \int \mathcal{D}U_j\ e^{-S_{\mathrm{LQCD}}} = e^{-S_F^{(\tau)}}\int \mathcal{D}U_j\ e^{-S_F^{(s)}-S_G} \\ &= e^{-S_F^{(\tau)}-S^{(s)}_{\mathrm{SCL}}}\left\langle e^{-S_G}\right\rangle \ . \end{aligned} \qquad (2\cdot7)$$

We have defined an expectation value as

$$\langle\mathcal{O}\rangle = \frac{1}{Z^{(s)}_{\mathrm{SCL}}}\int \mathcal{D}U_j\ \mathcal{O}[U_j]\ e^{-S_F^{(s)}} \ , \quad Z^{(s)}_{\mathrm{SCL}} = \int \mathcal{D}U_j\ e^{-S_F^{(s)}} = e^{-S^{(s)}_{\mathrm{SCL}}} \ . \qquad (2\cdot8)$$

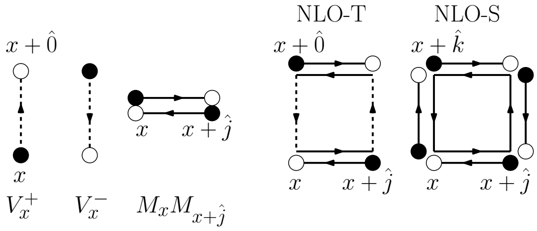

Fig. 1. Diagrams contributing to the SCL and NLO effective actions. Quarks (anti-quarks) are shown in open (filled) circles, and spatial (temporal) link variables are represented by solid (dashed) lines. Note that we should also take account of hermite conjugate contributions for NLO diagrams.

The factor $1/Z_{\mathrm{SCL}}^{(s)}$ ensures the normalization property $\langle \mathbf{1} \rangle = 1$. In order to systematically evaluate the effective action terms in each order of $1/g^2$, the cumulant (or coupled cluster) expansion is indispensable. It is well known that the expectation value of the exponential form operator with a small factor (*i.e.* $1/g^2$) can be evaluated by using the cumulant expansion[44)]

$$\left\langle e^{-S_G} \right\rangle = \sum_{n=0}^{\infty} \frac{(-1)^n}{n!} \left\langle {S_G}^n \right\rangle = \exp\left[\sum_{n=1}^{\infty} \frac{(-1)^n}{n!} \left\langle S_G^n \right\rangle_c \right] . \tag{2·9}$$

The correlation part in the connected diagram contributions is shown by the bracket $\langle \cdots \rangle_c$, and is called a cumulant, e.g. $\langle S_G^2 \rangle_c = \langle S_G^2 \rangle - \langle S_G \rangle^2$. By substituting Eq. (2·9) into Eq. (2·7), we find that the effective action is obtained as

$$\begin{aligned} S_{\mathrm{eff}} =& S_{\mathrm{SCL}} - \sum_{n=1}^{\infty} \frac{(-1)^n}{n!} \left\langle S_G^n \right\rangle_c \\ =& S_{\mathrm{SCL}} + \Delta S_{\mathrm{NLO}} + \Delta S_{\mathrm{NNLO}} + \mathcal{O}(1/g^6, 1/\sqrt{d}) \ . \end{aligned} \tag{2·10}$$

The n-th term in the sum is proportional to $1/g^{2n}$, and we can identify $n = 1$ and $n = 2$ terms as NLO and NNLO effective action, ΔS_{NLO} and ΔS_{NNLO}, and S_{SCL} shows the SCL effective action.

The SCL and NLO effective actions are known as,[18),34)]

$$S_{\mathrm{SCL}} = S_F^{(\tau)} + S_F^{(s)} = S_F^{(\tau)} - \frac{1}{4N_c} \sum_{x,j>0} M_x M_{x+\hat{j}} \ , \tag{2·11}$$

$$\begin{aligned} \Delta S_{\mathrm{NLO}} = \langle S_G \rangle_c =& \frac{1}{4N_c^2 g^2} \sum_{x,j>0} \left[V_x^+ V_{x+\hat{j}}^- + V_{x+\hat{j}}^+ V_x^- \right] \\ & -2 \times \frac{1}{16 N_c^4 g^2} \sum_{x,k>j>0} M_x M_{x+\hat{j}} M_{x+\hat{k}+\hat{j}} M_{x+\hat{k}} \ . \end{aligned} \tag{2·12}$$

The factor and sign of each term is summarized in Table I. The factor "2" in the last line accounts for the hermite conjugate contribution. In Fig. 1, we show the diagrams contributing to the SCL and NLO effective actions. The first three diagrams represent the temporal hopping ($S_F^{(\tau)}$) terms and the spatial meson hopping (MM) terms in S_{SCL}. The fourth and fifth diagrams show VV and $MMMM$ terms in ΔS_{NLO}.

2.3. *NNLO effective action*

From Eq. (2·10), we find that the NNLO effective action is given as the cumulant of S_G^2.

$$\begin{aligned}\Delta S_{\mathrm{NNLO}} &= -\frac{1}{2}\langle S_G^2\rangle_c = -\frac{1}{2}\left[\langle S_G^2\rangle - \langle S_G\rangle^2\right] \\ &= -\frac{1}{2g^4}\sum_{P,P'}\left[\langle U_P U_{P'}\rangle - \langle U_P\rangle\langle U_{P'}\rangle\right] \ , \qquad (2\cdot 13)\end{aligned}$$

where $U_P = \mathrm{tr}U_{\mu\nu,x}$ denotes the trace in the color space of a plaquette, or its conjugate. In the case where the two plaquettes (P and P') do not have any common spatial link variables, the average of the product is factorized as $\langle U_P U_{P'}\rangle = \langle U_P\rangle\langle U_{P'}\rangle$, which cancels with the second term. Thus only the connected diagrams can contribute to the NNLO effective action. In Fig. 2, we show the two plaquette configurations, where the plaquettes share at least one spatial link.

For a given two plaquette configuration, we consider the leading order terms in the $1/d$ expansion.[30] The sum over spatial directions $\sum_j$ in Eq. (2·11) would give rise to a factor d due to the spatial isotropy. Provided that the meson hopping term $\sum_j M_x M_{x+\hat{j}}$ in the SCL effective action stays finite at large d, the quark field $(\chi, \bar{\chi})$ should scale as $d^{-1/4}$. Then a factor d from the sum over spatial directions and a factor $1/d$ from the four quark fields cancel, and the mesonic hopping term $\sum_j M_x M_{x+\hat{j}}$ is found to be $\mathcal{O}(1/d^0)$, which is the leading order in the $1/d$ expansion. This also applies to the NNLO diagrams. For example, we consider the product of the same temporal plaquette, NNLO-TT1 in Fig. 2: We will have a factor d for the sum over the temporal plaquette $U_{0j,x}$, and four quark fields give rise to a factor $1/d$. Thus the diagram NNLO-TT1 in Fig. 2 is in the leading order $\mathcal{O}(1/d^0)$ in the $1/d$ expansion. Diagrams with more quarks for the same plaquette configuration are suppressed as $\mathcal{O}(1/\sqrt{d})$ for $N_c \geq 3$. This is called the systematic large dimensional or $1/d$ expansion.

Since we concentrate on the leading order terms in the $1/d$ expansion, we find that it is sufficient to consider the diagrams shown in Fig. 2, each of which includes the minimal number of quark fields for each plaquette configuration. We omit two plaquette configurations with $U_P = U_{P'}^\dagger$, which lead to a constant in the effective action in the leading order of the $1/d$ expansion, $\mathcal{O}(1/d^0)$. By utilizing the group integral formulae Eq. (2·6), these contributions lead to the following effective action terms

$$\begin{aligned}\Delta S_{\mathrm{NNLO}}^{(\tau\tau)} =& \frac{1}{8N_c^2 g^4}\sum_{x,j>0}\left[V_x^+ V_{x+\hat{j}}^- + V_{x+\hat{j}}^+ V_x^-\right] \\ &-\frac{1}{4N_c^3 g^4}\sum_{x,j>0}\left[W_x^+ W_{x+\hat{j}}^- + W_{x+\hat{j}}^+ W_x^-\right] \ , \qquad (2\cdot 14)\end{aligned}$$

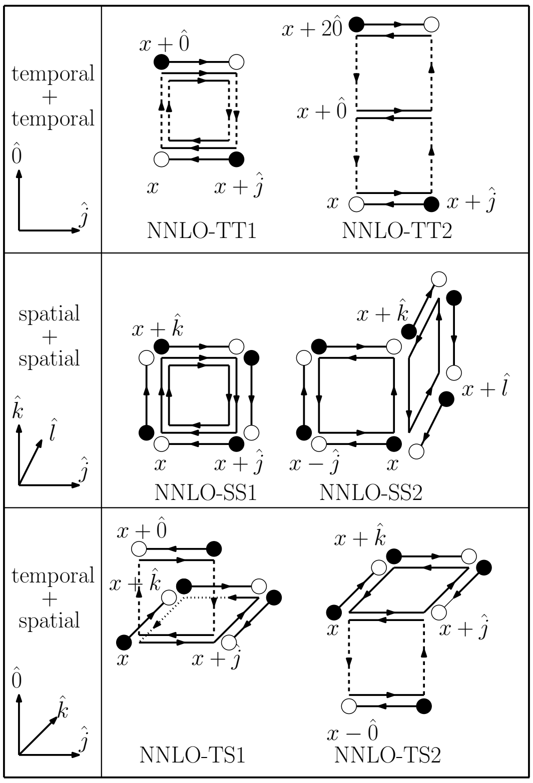

Fig. 2. Diagrams contributing to the NNLO effective action. Definitions of the symbols and lines are the same as those in Fig. 1. The top, middle and bottom rows represent the NNLO diagrams composed of the temporal-temporal, spatial-spatial, and temporal-spatial plaquette configurations, respectively.

$$\begin{aligned}
\mathit{\Delta} S^{(ss)}_{\rm NNLO} =& -2 \times \frac{1}{32 N_c^4 g^4} \sum_{x,k>j>0} \Big[M_x M_{x+\hat{j}} M_{x+\hat{j}+\hat{k}} M_{x+\hat{k}} \Big] \\
& - \frac{1}{64 N_c^7 g^4} \sum_{k>0,\ |j|\neq k,\ |l|\neq |j|,k} M_x M_{x+\hat{l}} M_{x+\hat{l}+\hat{k}} M_{x+\hat{k}} M_{x+\hat{k}-\hat{j}} M_{x-\hat{j}}\ , \qquad (2\cdot15)
\end{aligned}$$

$$\begin{aligned}
\mathit{\Delta} S^{(\tau s)}_{\rm NNLO} =& \frac{1}{16 N_c^5 g^4} \sum_{x,j>0,|k|\neq j} \left[V^+_x V^-_{x+\hat{j}} + V^+_{x+\hat{j}} V^-_x + V^+_{x-\hat{0}+\hat{j}} V^-_{x-\hat{0}} + V^+_{x-\hat{0}} V^-_{x-\hat{0}+\hat{j}} \right] \\
& \times M_{x+\hat{j}+\hat{k}} M_{x+\hat{k}}\ . \qquad (2\cdot16)
\end{aligned}$$

The factor "2" in the first line of $\mathit{\Delta} S^{(ss)}_{\rm NNLO}$ accounts for the hermite conjugate contribution. We find that two new mesonic composites appear

$$W^+_x = \bar{\chi}_x e^{2\mu} U_{0,x} U_{0,x+\hat{0}} \chi_{x+2\hat{0}}\ , \quad W^-_x = \bar{\chi}_{x+2\hat{0}} e^{-2\mu} U^\dagger_{0,x+\hat{0}} U^\dagger_{0,x} \chi_x\ . \qquad (2\cdot17)$$

These composite connect the quark fields in the next-to-nearest neighboring (NNN) temporal sites. In Fig. 2, the top, second and bottom rows represent $\mathit{\Delta} S^{(\tau\tau)}_{\rm NNLO}$,

Table I. The factors and sign which come from, (A) a global NNLO factor $1/g^0$, $1/g^2$ or $1/g^4$, (B) a symmetric factor (Sym.) 1/2 for the product of two same plaquettes, (C) product of factors $-1/2$ and $1/2$ for the forward $(\bar{\chi}U\chi)$ and backward $(\bar{\chi}U^{\dagger}\chi)$ fermionic elements (F.E.), (D) a product of the staggered factors $\eta_{j,x}$, and (E) one-link integrals. Each entry in the left column represents a diagram shown in Fig. 1 and 2.

	(A) Global	(B) Sym.	(C) F.E.	(D) $\eta_{j,x}$	(E) U_j	Total
SCL-S	$1/g^0$	1	$-(1/2)^2$	+1	$1/N_c$	$-1/4N_c$
NLO-T	$1/g^2$	1	$-(1/2)^2$	−1	$1/N_c^2$	$+1/4N_c^2g^2$
NLO-S	$1/g^2$	1	$+(1/2)^4$	−1	$1/N_c^4$	$-1/16N_c^4g^2$
NNLO-TT1	$1/g^4$	1/2	$-(1/2)^2$	−1	$1/N_c^2$	$+1/8N_c^2g^4$
NNLO-TT2	$1/g^4$	1	$-(1/2)^2$	+1	$1/N_c^3$	$-1/4N_c^3g^4$
NNLO-SS1	$1/g^4$	1/2	$+(1/2)^4$	−1	$1/N_c^4$	$-1/32N_c^4g^4$
NNLO-SS2	$1/g^4$	1	$-(1/2)^6$	+1	$1/N_c^7$	$-1/64N_c^7g^4$
NNLO-TS1,2	$1/g^4$	1	$+(1/2)^4$	+1	$1/N_c^5$	$+1/16N_c^5g^4$

$\varDelta S^{(ss)}_{\rm NNLO}$ and $\varDelta S^{(\tau s)}_{\rm NNLO}$, respectively. Note that for diagrams which include quarks, we also consider the hermite conjugate of those diagrams.

We summarize the factor and sign in SCL, NLO and NNLO in Table I. The factor and sign of each term is a product of (A) a global NNLO factor $1/g^0$, $1/g^2$ or $1/g^4$, (B) a symmetric factor 1/2 for the product of two same plaquettes, (C) product of factors $-1/2$ and $1/2$ for the forward $(\bar{\chi}U\chi)$ and backward $(\bar{\chi}U^{\dagger}\chi)$ fermionic elements, (D) product of the staggered factors $\eta_{j,x}$, and (E) a factor from the one-link integral. Expressing the effective action as a function of color singlet composites M, V and W, we generally obtain a factor "−1" resulting from an odd number times of grassmann number exchanges. This sign factor is taken care in the global factor and shown in the column (A) of Table I. For a product of different plaquettes (P, P'), there are two combinations (P, P') and (P', P) in the sum of Eq. (2·13), and they give rise to a factor 2. With the factor $-1/2g^4$ found in Eq. (2·13), we get a global factor $1/g^4$. For a product of the same plaquettes $P = P'$ in NNLO-TT1 and NNLO-SS1, we need a symmetric factor 1/2. The factor from the one-link integral is $1/N_c^k$, where k is the number of integrated out spatial links. Also in the case to use the second formula in Eq. (2·6), we have $1/N_c$ in the present configurations. For example, in NNLO-TT1, we have a factor $1/(N_c!)^2$ from the spatial link integrals, and the following combination of temporal link variables remains on the link $(0, x+\hat{j})$

$$\varepsilon_{a_1b_1\cdots c_1}\varepsilon_{a_2b_2\cdots c_2}U^{b_1b_2}_{0,x+\hat{j}}\cdots U^{c_1c_2}_{0,x+\hat{j}} = (N_c-1)! \times U^{\dagger\, a_2a_1}_{0,x+\hat{j}} \ . \qquad (2\cdot 18)$$

We also find another $(N_c - 1)!$ appears on the link $(0, x)$, and the factor from the one-link integral is found to be $1/N_c^2$. In a similar way, $1/N_c^4$ appears for NNLO-SS1. Note that NLO-S and NNLO-SS1 action terms are hermite, hence one find a factor 2 in $MMMM$ terms of Eq. (2·12) and (2·15).

We explain the factor and sign for NNLO-TS1, as an example. There are two forward $((k, x)$ and $(j, x+\hat{k}))$ and two backward $((k, x+\hat{j})$ and $(j, x+\hat{0}))$ fermionic elements, and we have a factor $+(1/2)^4$. Staggered factors for these elements are $\eta_{k,x}$, $\eta_{j,x+\hat{k}} = \alpha\eta_{j,x}$, $\eta_{k,x+\hat{j}} = -\alpha\eta_{k,x}$ and $\eta_{j,x+\hat{0}} = -\eta_{j,x}$, where $\alpha = 1$ (-1) for $k > j$ $(k < j)$. The product of these staggered factors results in $+1$. Five spatial links are integrated out, and give a factor $1/N_c^5$. Together with the global factor $1/g^4$, we find the coefficient $+1/16N_c^5 g^4$ for NNLO-TS1.

We combine those terms in NLO and NNLO having the same composites. Now we have obtained the effective action S_{eff} in Eq. (2·10) up to $\mathcal{O}(1/g^6, 1/\sqrt{d})$

$$S_{\text{eff}} = S_{\text{SCL}} + \mathit{\Delta}S^{\tau} + \mathit{\Delta}S^{s} + \mathit{\Delta}S^{\tau\tau} + \mathit{\Delta}S^{ss} + \mathit{\Delta}S^{\tau s} \tag{2·19a}$$

$$= \frac{1}{2}\sum_{x}(V_x^{+} - V_x^{-}) - \frac{b_\sigma}{2d}\sum_{x,j>0}[MM]_{j,x} \tag{2·19b}$$

$$+ \frac{1}{2}\,\frac{\beta_\tau}{2d}\sum_{x,j>0}[V^{+}V^{-} + V^{-}V^{+}]_{j,x} \tag{2·19c}$$

$$- \frac{1}{2}\,\frac{\beta_s}{d(d-1)}\sum_{x,j>0,k>0,k\neq j}[MMMM]_{jk,x} \tag{2·19d}$$

$$- \frac{\beta_{\tau\tau}}{2d}\sum_{x,j>0}[W^{+}W^{-} + W^{-}W^{+}]_{j,x} \tag{2·19e}$$

$$- \frac{\beta_{ss}}{4d(d-1)(d-2)}\sum_{\substack{x,\,j>0,\,|k|>0,\,|l|>0\\ |k|\neq j,\,|l|\neq j,\,|l|\neq|k|}}[MMMM]_{jk,x}[MM]_{j,x+\hat{l}} \tag{2·19f}$$

$$+ \frac{\beta_{\tau s}}{8d(d-1)}\sum_{x,j>0,|k|\neq j}[V^{+}V^{-} + V^{-}V^{+}]_{j,x}\left([MM]_{j,x+\hat{k}} + [MM]_{j,x+\hat{k}+\hat{0}}\right)\ . \tag{2·19g}$$

We have introduced a short-hand notation

$$[AB]_{j,x} = A_x B_{x+\hat{j}}\ ,\quad [ABCD]_{jk,x} = A_x B_{x+\hat{j}} C_{x+\hat{j}+\hat{k}} D_{x+\hat{k}}\ . \tag{2·20}$$

We obtain Eq. (2·19g) by shifting x to $x + \hat{0}$ in the third and fourth $V^{+}V^{-}$ terms in Eq. (2·16). NLO and NNLO effective action terms, $\mathit{\Delta}S^{K}(K = \tau, s, \tau\tau, ss, \tau s)$, correspond to Eqs. (2·19c)–(2·19g). The coefficients are defined as

$$b_\sigma = \frac{d}{2N_c}\ ,\quad \beta_\tau = \frac{d}{N_c^2 g^2}\left(1 + \frac{1}{2g^2}\right)\ ,\quad \beta_s = \frac{d(d-1)}{8N_c^4 g^2}\left(1 + \frac{1}{2g^2}\right)\ , \tag{2·21}$$

$$\beta_{\tau\tau} = \frac{d}{2N_c^3 g^4}\ ,\quad \beta_{ss} = \frac{d(d-1)(d-2)}{16N_c^7 g^4}\ ,\quad \beta_{\tau s} = \frac{d(d-1)}{2N_c^5 g^4}\ . \tag{2·22}$$

2.4. *Extended Hubbard-Stratonovich transformation*

The effective action S_{eff} derived in the previous subsection contains several types of composite products, which include many fermion fields. In order to perform the grassmann integral, it is much more convenient to reduce these higher order terms to the spatially local and bilinear form in the fermion fields through the bosonization procedure, so-called the Hubbard-Stratonovich (HS) transformation. The standard HS transformation is applicable to the product of composites of similar kind, while

Table II. The application of the Extended Hubbard-Stratonovich transformation to effective action terms.

		α	A	B
$\Delta S^{\tau\tau}$	(2·19e)	$\beta_{\tau\tau}/2d$	W_x^+	W_{x+j}^-
ΔS^{ss}	(2·19f)	$\beta_{ss}/4d(d-1)(d-2)$	$[MM]_{j,x+\hat{l}}$	$[MMMM]_{jk,x}$
$\Delta S^{\tau s}$	(2·19g)	$\beta_{\tau s}/8d(d-1)$	$-[V^+V^-]_{j,x}$	$[MM]_{j,x+\hat{k}} + [MM]_{j,x+\hat{k}+\hat{0}}$
$\Delta\tilde{S}^{\tau}$	(2·29)	$(\beta_\tau + \beta_{\tau s}\psi_{\tau s})/4d$	$-V_x^+$	$V_{x+\hat{j}}^-$
$\Delta\tilde{S}^{s}$	(2·30)	$(\beta_s + 2\beta_{ss}\bar{\psi}_{ss})/2d(d-1)$	$[MM]_{j,x}$	$[MM]_{j,x+\hat{k}}$

NLO and NNLO terms contain the product of different types, such as V^+V^-. In order to treat these terms, we apply the extended Hubbard-Stratonovich (EHS) transformation,[34),35)] where two auxiliary fields (φ, ϕ) are introduced simultaneously

$$e^{\alpha AB} = \int d\varphi\, d\phi\, e^{-\alpha\left\{[\varphi-(A+B)/2]^2+[\phi-i(A-B)/2]^2\right\}+\alpha AB}$$

$$\approx e^{-\alpha\left\{\varphi^2-(A+B)\varphi+\phi^2-i(A-B)\phi\right\}}\Big|_{\text{stationary}} \tag{2·23}$$

$$\approx e^{-\alpha\left\{\bar{\psi}\psi-A\psi-\bar{\psi}B\right\}}\Big|_{\text{stationary}} , \tag{2·24}$$

where α is an arbitrary positive real constant. In the second line, we approximate the integral by the integrand at the stationary values, $\varphi = \langle A+B\rangle/2$ and $\phi = i\langle A-B\rangle/2$ (the saddle point approximation). This procedure is denoted by "$\approx$", and we use this notation in later discussions. In the last line Eq. (2·24), we have performed the transformation $\psi = \varphi + i\phi$ and $\bar{\psi} = \varphi - i\phi$. When $A = B$ is satisfied, Eq. (2·23) is equivalent to the standard HS transformation. In the case where both $\langle A\rangle$ and $\langle B\rangle$ are real, the stationary value of ϕ is pure imaginary. Thus we replace $\phi \to i\omega$ in Eq. (2·23), then the stationary value of ω is real

$$e^{\alpha AB} \approx e^{-\alpha\left\{\varphi^2-(A+B)\varphi-\omega^2+(A-B)\omega\right\}}\Big|_{\text{stationary}} . \tag{2·25}$$

We first apply the EHS transformation in the complex representation, Eq. (2·24), to NNLO terms in S_{NNLO}, Eqs. (2·19e), (2·19f) and (2·19g). By substituting (α, A, B) in Eq. (2·24) as shown in Table II, we obtain

$$\begin{aligned}\Delta S^{\tau\tau} \approx& \frac{\beta_{\tau\tau}}{2d}\sum_{x,j>0}\left[\bar{\psi}_{\tau\tau}\psi_{\tau\tau} - W_x^+\psi_{\tau\tau} - \bar{\psi}_{\tau\tau}W_{x+\hat{j}}^-\right] + (x \leftrightarrow x+\hat{j})\\ \simeq& N_\tau L^d\beta_{\tau\tau}\bar{\psi}_{\tau\tau}\psi_{\tau\tau} - \beta_{\tau\tau}\sum_x(\psi_{\tau\tau}W_x^+ + \bar{\psi}_{\tau\tau}W_x^-) ,\end{aligned} \tag{2·26}$$

$$\begin{aligned}\Delta S^{ss} \approx& \frac{\beta_{ss}}{4d(d-1)(d-2)}\sum_{\substack{x,\,j>0,\,|k|>0,\,|l|>0\\ |k|\neq j,\,|l|\neq j,\,|l|\neq|k|}}\left[\bar{\psi}_{ss}\psi_{ss} - [MM]_{j,x+\hat{l}}\,\psi_{ss} - \bar{\psi}_{ss}[MMMM]_{jk,x}\right]\\ \simeq& N_\tau L^d\beta_{ss}\bar{\psi}_{ss}\psi_{ss} - \frac{\beta_{ss}}{d}\psi_{ss}\sum_{x,j>0}[MM]_{j,x} - \frac{\beta_{ss}\bar{\psi}_{ss}}{d(d-1)}\sum_{x,j>0,k>0,k\neq j}[MMMM]_{jk,x}\end{aligned} \tag{2·27}$$

$$\begin{aligned}
\mathit{\Delta} S^{\tau s} \approx& \frac{\beta_{\tau s}}{8d(d-1)} \sum_{x,j>0,|k|\neq j} \Big[\bar{\psi}_{\tau s}\psi_{\tau s} + [V^+V^-]_{j,x}\psi_{\tau s} \\
&\qquad\qquad -\bar{\psi}_{\tau s}([MM]_{j,x+\hat{k}} + [MM]_{j,x+\hat{k}+\hat{0}})\Big] + (x \leftrightarrow x+\hat{j}) \\
\simeq& N_\tau L^d \frac{\beta_{\tau s}}{2}\bar{\psi}_{\tau s}\psi_{\tau s} + \frac{\beta_{\tau s}}{4d}\psi_{\tau s}\sum_{x,j>0}[V^+V^- + V^-V^+]_{j,x} - \frac{\beta_{\tau s}}{d}\bar{\psi}_{\tau s}\sum_{x,j>0}[MM]_{j,x}\ ,
\end{aligned} \tag{2·28}$$

We have introduced the auxiliary fields $(\bar{\psi}_K, \psi_K)$ in $\mathit{\Delta} S^K$ ($K = \tau\tau, \tau s, ss$). In Eq. (2·26)-(2·28), the symbol "$\simeq$" represents that constant and isotropic values are assumed for auxiliary fields $(\bar{\psi}_K, \psi_K)$, and we use this notation in later discussions. Note that the EHS transformation is applied so that the auxiliary fields $(\bar{\psi}_{ss}, \psi_{ss}, \bar{\psi}_{\tau s}, \psi_{\tau s})$ have no chiral charge in Eqs. (2·27) and (2·28). For example, in Eq. (2·27), we have decomposed the six-meson term $(MMMMMM)$ into MM and $MMMM$ mesonic terms, and introduced auxiliary fields for their composites, $(\bar{\psi}_{ss}, \psi_{ss}) = (\langle MM\rangle, \langle MMMM\rangle)$.

NNLO contributions in Eqs. (2·27) and (2·28) generate terms, $[V^+V^- + V^-V^+]$ and $[MMMM]$. They can be absorbed into the NLO contributions, Eqs. (2·19c) and (2·19d). We put $[V^+V^- + V^-V^+]$ and $[MMMM]$ terms in NLO and NNLO together and bosonize as

$$\begin{aligned}
\mathit{\Delta}\tilde{S}^{\tau} =& \frac{\beta_\tau + \beta_{\tau s}\psi_{\tau s}}{4d}\sum_{x,j>0}[V^+V^- + V^-V^+]_{j,x} \\
\approx& \frac{\beta'_\tau}{4d}\sum_{x,j>0}\Big[\bar{\psi}_\tau\psi_\tau + V^+_x\psi_\tau - \bar{\psi}_\tau V^-_{x+\hat{j}}\Big] + (x \leftrightarrow x+\hat{j}) \\
\simeq& N_\tau L^d \frac{\beta'_\tau}{2}\bar{\psi}_\tau\psi_\tau + \frac{\beta'_\tau}{2}\sum_x(\psi_\tau V^+_x - \bar{\psi}_\tau V^-_x)\ ,
\end{aligned} \tag{2·29}$$

$$\begin{aligned}
\mathit{\Delta}\tilde{S}^{s} =& -\frac{\beta_s + 2\beta_{ss}\bar{\psi}_{ss}}{2d(d-1)}\sum_{x,j>0,k>0,k\neq j}[MMMM]_{jk,x} \\
\approx& \frac{\beta'_s}{2d(d-1)}\sum_{x,j>0,k>0,k\neq j}\Big[\bar{\psi}_s\psi_s - [MM]_{j,x}\psi_s - \bar{\psi}_s[MM]_{j,x+\hat{k}}\Big] \\
\simeq& N_\tau L^d \frac{\beta'_s}{2}\bar{\psi}_s\psi_s - \frac{\beta'_s}{2d}\sum_{x,j>0}(\psi_s + \bar{\psi}_s)[MM]_{j,x}\ ,
\end{aligned} \tag{2·30}$$

where $\beta'_\tau = \beta_\tau + \beta_{\tau s}\psi_{\tau s}$ and $\beta'_s = \beta_s + 2\beta_{ss}\bar{\psi}_{ss}$. We find that V^+V^- and $MMMM$ terms shifts the coefficients of SCL effective action terms via EHS transformations. In previous NLO investigations,[34),35)] we have developed the method to express V^+V^- and $MMMM$ effects as modifications of the wave function renormalization factor, quark mass and chemical potential. In the present investigation, we need to manipulate the next-to-nearest neighboring interaction come from $W^\pm$ effects in Eq. (2·26) before utilizing those techniques developed in NLO. The $W^\pm$ effects are evaluated in the next subsection.

We introduce the chiral condensate auxiliary field σ by using the standard HS transformation. We combine the mesonic hopping $[MM]$ terms in S_{SCL} (Eq. (2·19b)), NNLO contributions (Eqs. (2·27) and (2·28)), and NLO contributions with NNLO effects (Eq. (2·30)). Then we obtain the modified mesonic hopping terms, which can be bosonized as

$$\begin{aligned}
-\frac{b'_\sigma}{2}\sum_{x,y} M_x V_{xy} M_y \approx & b'_\sigma \sum_{x,y}\left[\frac{1}{2}\sigma_x V_{xy}\sigma_y + \sigma_x V_{xy} M_y\right] \\
\simeq & N_\tau L^d\,\frac{b'_\sigma}{2}\sigma^2 + b'_\sigma \sigma \sum_x M_x \ , && (2\cdot31) \\
b'_\sigma = & b_\sigma + 2\left[\beta_{ss}\psi_{ss} + \beta_{\tau s}\bar{\psi}_{\tau s} + (\beta_s + 2\beta_{ss}\bar{\psi}_{ss})(\psi_s + \bar{\psi}_s)\right] \ , && (2\cdot32) \\
V_{xy} = & \frac{1}{2d}\sum_j (\delta_{x+\hat{j},y} + \delta_{x-\hat{j},y}) \ . && (2\cdot33)
\end{aligned}$$

We have obtained the additional mass term $b'_\sigma \sigma \sum_x M_x$. Combined with the current quark mass m_0, we obtain a constituent quark mass as

$$m_q = b'_\sigma \sigma + m_0 \ . \qquad (2\cdot34)$$

Now we have the NNLO effective action in the spatially local and bilinear form in the fermion fields. We collect all the remaining terms from S_{SCL} (Eq. (2·19b)), NNLO terms (Eqs. (2·26), (2·27) and (2·28)), NLO terms (Eqs. (2·29) and (2·30)), and the chiral condensate term (Eq. (2·31))

$$\begin{aligned}
S_{\mathrm{eff}} = & S^{(F)}_{\mathrm{eff}} + S^{(X)}_{\mathrm{eff}} \ , && (2\cdot35) \\
S^{(F)}_{\mathrm{eff}} = & \frac{1}{2}\sum_x \left[C V^+_x - \bar{C} V^-_x\right] + \sum_x m_q M_x - \beta_{\tau\tau}\sum_x (\psi_{\tau\tau} W^+_x + \bar{\psi}_{\tau\tau} W^-_x) \ , && (2\cdot36) \\
C = & 1 + (\beta_\tau + \beta_{\tau s}\psi_{\tau s})\psi_\tau \ , \ \bar{C} = 1 + (\beta_\tau + \beta_{\tau s}\psi_{\tau s})\bar{\psi}_\tau \ , && (2\cdot37) \\
S^{(X)}_{\mathrm{eff}} = & N_\tau L^d \left[\beta_{\tau\tau}\bar{\psi}_{\tau\tau}\psi_{\tau\tau} + \beta_{ss}\bar{\psi}_{ss}\psi_{ss} + \frac{1}{2}\beta_{\tau s}\bar{\psi}_{\tau s}\psi_{\tau s} + \frac{1}{2}(\beta_\tau + \beta_{\tau s}\psi_{\tau s})\bar{\psi}_\tau\psi_\tau \right. \\
& \left. + \frac{1}{2}(\beta_s + 2\beta_{ss}\bar{\psi}_{ss})\bar{\psi}_s\psi_s + \frac{1}{2}b'_\sigma\,\sigma^2\right] \ , && (2\cdot38)
\end{aligned}$$

where $S^{(F)}_{\mathrm{eff}}$ and $S^{(X)}_{\mathrm{eff}}$ represent those effective action terms with and without fermions, respectively. The SCL and NLO effective action contains V^+_x, V^-_x and M_x, and their corresponding effective potentials are known.[34)] In order to obtain the effective potential from the NNLO effective action containing W^+_x and W^-_x in addition to V^+_x, V^-_x and M_x, we discuss how to treat W^+_x, W^-_x terms in the next subsection.

2.5. *Gluonic dressed fermion*

The fermionic NNLO effective action $S^{(F)}_{\mathrm{eff}}$ in Eq. (2·36) is in the spatially local and bilinear form of χ and $\bar{\chi}$, then it is possible to obtain the fermion determinant analytically in the form of Matsubara product. In order to evaluate the Matsubara product, we need to obtain the Matsubara frequency which gives zero determinant.

Because of the coupling of the next-to-nearest neighboring (NNN) temporal sites via W^+ and W^-, the fermion matrix becomes pentadiagonal rather than tridiagonal and it is not easy to obtain the solution. In the present case, NNN terms are in the $\mathcal{O}(1/g^4)$, then we can absorb them by introducing a gluonic dressed fermion

$$\chi'_x = \chi_x + Ae^{\mu}U_{0,x}\,\chi_{x+\hat{0}} \ , \quad \bar{\chi}'_x = \bar{\chi}_x + \bar{A}\bar{\chi}_{x+\hat{0}}e^{-\mu}U^\dagger_{0,x} \ , \tag{2·39}$$

where $A = \mathcal{O}(1/g^4)$. Mesonic composites are represented in this dressed fermion as

$$M_x = M'_x - AV'^+_x - \bar{A}V'^-_x + \mathcal{O}(1/g^8) \ , \tag{2·40}$$
$$V^+_x = V'^+_x - \bar{A}M'_{x+\hat{0}} - AW'^+_x + \mathcal{O}(1/g^8) \ , \tag{2·41}$$
$$V^-_x = V'^-_x - AM'_{x+\hat{0}} - \bar{A}W'^-_x + \mathcal{O}(1/g^8) \ , \tag{2·42}$$
$$W^+_x = W'^+_x + \mathcal{O}(1/g^8) \ , \quad W^-_x = W'^-_x + \mathcal{O}(1/g^8) \ , \tag{2·43}$$

where primed composites denote those with dressed fermions, such as $M'_x = \bar{\chi}'_x\chi'_x$. In terms of this dressed fermion, the fermionic term $S^{(F)}_{\text{eff}}$ is rewritten as

$$\begin{aligned} S^{(F)}_{\text{eff}} =& \frac{1}{2}\sum_x \left[(C - 2m_qA)V'^+_x - (\bar{C} + 2m_q\bar{A})V'^-_x\right] + \sum_x \left[m_q - \frac{1}{2}(C\bar{A} - \bar{C}A)\right] M'_x \\ & -\frac{1}{2}\sum_x \left[(2\beta_{\tau\tau}\psi_{\tau\tau} + CA)W'^+_x + (2\beta_{\tau\tau}\bar{\psi}_{\tau\tau} - \bar{C}\bar{A})W'^-_x\right] + \mathcal{O}(1/g^8) \ . \end{aligned} \tag{2·44}$$

We find that NNN terms in the primed fields cancel with each other when we choose $A = -2\beta_{\tau\tau}\psi_{\tau\tau}/C$ and $\bar{A} = 2\beta_{\tau\tau}\bar{\psi}_{\tau\tau}/\bar{C}$. Then the NNLO fermionic effective action is represented in V'^+_x, V'^-_x and M'_x terms. In the later discussion, we regard χ' and $\bar{\chi}'$ as quarks and anti-quarks, and omit the prime for the mesonic composites. The fermionic effective action now reads

$$S^{(F)}_{\text{eff}} = \frac{1}{2}\sum_x \left[Z_- V^+_x - Z_+ V^-_x\right] + \sum_x m'_q M_x + \mathcal{O}(1/g^6) \ , \tag{2·45}$$

$$\begin{aligned} Z_- =& C - 2m_qA = C + 4m'_q\beta_{\tau\tau}\psi_{\tau\tau} + \mathcal{O}(1/g^6) \ , \\ Z_+ =& \bar{C} + 2m_q\bar{A} = \bar{C} + 4m'_q\beta_{\tau\tau}\bar{\psi}_{\tau\tau} + \mathcal{O}(1/g^6) \ , \end{aligned} \tag{2·46}$$

$$m'_q = m_q - \frac{1}{2}(C\bar{A} - \bar{C}A) = m_q - \beta_{\tau\tau}(\psi_{\tau\tau} + \bar{\psi}_{\tau\tau}) + \mathcal{O}(1/g^6) \ . \tag{2·47}$$

Comparing Eq. (2·45) with (2·36), we find that the effects of $W^\pm$ are expressed as modifications of the constituent quark mass and the coefficient of $V^\pm$ through the gluonic dressed fermion. It should be noted that the Jacobian between $(\chi, \bar{\chi})$ and $(\chi', \bar{\chi}')$ deviates from unity by $\mathcal{O}(1/g^{4N_\tau N_c})$, and we can ignore its effects in NNLO SC-LQCD. As a result, NNLO effective action is represented in V^+_x, V^-_x and M_x terms as in the case of bosonized NLO effective action.[34),35)]

2.6. *Effective potential*

In the discussion by the previous subsection, we find that the NLO and NNLO corrections lead to the coefficient modification of V^+, V^- and M in the fermionic effective action. The meaning of this modification would be more clearly understood in the following representation of the fermionic effective action

$$\begin{aligned} S_{\text{eff}}^{(F)} =& \frac{1}{2}\sum_x \left[Z_- V_x^+ - Z_+ V_x^-\right] + \sum_x m'_q M_x \\ =& Z_\chi \left[\sum_{x,y} \frac{1}{2}\left[e^{-\delta\mu} V_x^+ - e^{\delta\mu} V_x^-\right] + \sum_x \tilde{m}_q M_x\right] \\ =& Z_\chi \sum_{xy} \bar{\chi}_x \, G_{xy}^{-1}(\tilde{m}_q;\tilde{\mu},T)\chi_y \ , \end{aligned} \tag{2·48}$$

$$G_{xy}^{-1}(\tilde{m}_q;\mu,T) = \frac{1}{2}\left[e^{\mu} U_{0,x}\,\delta_{x+\hat{0},y} - e^{-\mu} U_{0,x}^\dagger\,\delta_{x-\hat{0},y}\right] + \tilde{m}_q \delta_{xy} \ , \tag{2·49}$$

$$Z_\chi = \sqrt{Z_+ Z_-} \ , \quad \tilde{m}_q = \frac{m'_q}{Z_\chi} \ , \quad \tilde{\mu} = \mu - \delta\mu = \mu - \log\sqrt{Z_+/Z_-} \ . \tag{2·50}$$

In this form of the effective action, we easily find that NNLO effects result in the modification of the wave function renormalization factor Z_χ, quark mass $\tilde{m}_q$ and chemical potential $\tilde{\mu}$ by using the technique developed in NLO investigations.34),35)

We carry out the Grassmann integral over the quark fields and the temporal link integral in a standard way.16),18) First, we perform the Fourier transformation in the temporal coordinate, and obtain the product in the frequency by the Grassmann integral over the quark fields. Second, we evaluate the product in the frequency by using the Matsubara method. Finally, we carry out the temporal link integral by using the Haar measure. The fermionic part in the effective potential $\mathcal{F}_q$ is given as

$$\mathcal{F}_q \equiv -\frac{1}{N_\tau L^d}\log\left[\int \mathcal{D}[\chi,\bar{\chi},U_0] e^{-S_{\text{eff}}^{(F)}}\right] = \mathcal{V}_q(\tilde{m}_q;\tilde{\mu},T) - N_c \log Z_\chi \ , \tag{2·51}$$

$$\mathcal{V}_q(\tilde{m}_q;\tilde{\mu},T) = -T\log\left[\frac{\sinh[(N_c+1)E_q(\tilde{m}_q)/T]}{\sinh[E_q(\tilde{m}_q)/T]} + 2\cosh(N_c\tilde{\mu}/T)\right] \ , \tag{2·52}$$

where the number of temporal sites is replaced as $N_\tau = 1/T$, and $E_q(\tilde{m}_q) = \text{arcsinh}\,(\tilde{m}_q)$ is regarded as the quark excitation energy.

The latter point is understood from the expression of the temporal quark hopping matrix determinant,18)

$$e^{-\mathcal{V}_q L^d/T} = \int \mathcal{D}[U_0]\,\det{}_{x,c}\, G_{xy}^{-1}(\tilde{m}_q;\tilde{\mu},T) \tag{2·53}$$

$$= \prod_{\mathbf{x}} \int d\mathcal{U}_0 \,\det{}_c \left[e^{E_q/T}\left(1 + \mathcal{U}_0 e^{-(E_q-\tilde{\mu})/T}\right)\left(1 + \mathcal{U}_0^\dagger e^{-(E_q+\tilde{\mu})/T}\right)\right] \ , \tag{2·54}$$

where $\mathcal{U}_0(\mathbf{x}) = \prod_\tau U_0(\mathbf{x},\tau)$. We can evaluate this temporal link integral exactly, for example, in the Polyakov gauge,16)

$$U_0(\mathbf{x},\tau) = \text{diag}(e^{iT\theta_1(\mathbf{x})}, \cdots, e^{iT\theta_{N_c}(\mathbf{x})}) \ . \tag{2·55}$$

We find the Boltzmann factor $\exp\left[-(E_q \pm \tilde{\mu})/T\right]$ appears, and the integrand is nothing but the thermal quark contribution to the partition function if U_0 is close to unity. Note that the determinant is for the spacetime and color in Eq. (2·53), and for the color in Eq. (2·54).

We obtain the NNLO effective potential as follows.

$$\begin{aligned}
\mathcal{F}_{\text{eff}} \equiv& -\frac{1}{N_\tau L^d}\log\left[\int \mathcal{D}[\chi,\bar{\chi},U_0]e^{-S_{\text{eff}}^{(F)}-S_{\text{eff}}^{(X)}}\right]\\
=&\mathcal{F}_q(\varPhi;\mu,T)+\mathcal{F}_{\text{eff}}^{(X)}(\varPhi)\ , \qquad (2·56)\\
\mathcal{F}_{\text{eff}}^{(X)} =& S_{\text{eff}}^{(X)}/N_\tau L^d\\
=&\frac{1}{2}b'_\sigma\,\sigma^2+\frac{1}{2}(\beta_\tau+\beta_{\tau s}\psi_{\tau s})\,\bar{\psi}_\tau\psi_\tau+\frac{1}{2}(\beta_s+2\beta_{ss}\bar{\psi}_{ss})\bar{\psi}_s\psi_s\\
&+\beta_{\tau\tau}\bar{\psi}_{\tau\tau}\psi_{\tau\tau}+\beta_{ss}\bar{\psi}_{ss}\psi_{ss}+\frac{1}{2}\beta_{\tau s}\bar{\psi}_{\tau s}\psi_{\tau s}\ , \qquad (2·57)\\
\tilde{m}_q =& \frac{m'_q}{Z_\chi}\ , \quad m'_q=b'_\sigma\sigma+m_0-\beta_{\tau\tau}(\bar{\psi}_{\tau\tau}+\psi_{\tau\tau})\ , \qquad (2·58)\\
Z_+ =& 1+(\beta_\tau+\beta_{\tau s}\psi_{\tau s})\bar{\psi}_\tau+4\beta_{\tau\tau}m'_q\bar{\psi}_{\tau\tau}\ , \qquad (2·59)\\
Z_- =& 1+(\beta_\tau+\beta_{\tau s}\psi_{\tau s})\psi_\tau+4\beta_{\tau\tau}m'_q\psi_{\tau\tau}\ , \qquad (2·60)\\
b'_\sigma =& b_\sigma+(\beta_s+2\beta_{ss}\bar{\psi}_{ss})(\psi_s+\bar{\psi}_s)+2\beta_{ss}\psi_{ss}+2\beta_{\tau s}\bar{\psi}_{\tau s}\ , \qquad (2·61)
\end{aligned}$$

where $\varPhi=(\sigma,\{\psi_K,\bar{\psi}_K;K=\tau,s,\tau\tau,\tau s,ss\})$. Coupling constants $(b_\sigma,\beta_\tau,\beta_s,\beta_{\tau\tau},\beta_{\tau s},\beta_{ss})$ are defined in Eqs. (2·21) and (2·22).

2.7. *Stationary conditions*

The auxiliary fields introduced during the bosonization procedure have to satisfy the stationary condition, $\partial\mathcal{F}_{\text{eff}}/\partial\varPhi=0$. Within the constant field approximation, the stationary values of auxiliary fields are related with each other, then we replace the auxiliary fields other than (σ, $\bar{\psi}_\tau$ and ψ_τ) with their equilibrium values as functions of (σ, $\bar{\psi}_\tau$ and ψ_τ).

We can solve the stationary conditions for all auxiliary fields exactly. In solving the stationary condition, we first note that the quark free energy is a function of m'_q, Z_+ and Z_-, as we can guess from Eq. (2·45). Then the variation $\mathcal{F}_q$ is obtained as

$$\frac{\partial\mathcal{F}_q}{\partial\varPhi}=\frac{\partial\mathcal{F}_q}{\partial m'_q}\frac{\partial m'_q}{\partial\varPhi}+\frac{\partial\mathcal{F}_q}{\partial Z_+}\frac{\partial Z_+}{\partial\varPhi}+\frac{\partial\mathcal{F}_q}{\partial Z_-}\frac{\partial Z_-}{\partial\varPhi}\ . \qquad (2·62)$$

Since Z_+ and Z_- contain m'_q, the above derivative $\partial\mathcal{F}_q/\partial m'_q$ also contains the derivative via $Z_\pm$, $(\partial\mathcal{F}_q/\partial Z_\pm)(\partial Z_\pm/\partial m'_q)$. Substituting $\sigma,\psi_s,\bar{\psi}_s,\bar{\psi}_\tau,\psi_\tau$, in Eq. (2·62), the stationary conditions for these fields read,

$$\sigma=-\frac{\partial\mathcal{F}_q}{\partial m'_q}\ ,\quad \psi_s=\bar{\psi}_s=\sigma^2\ ,\quad \bar{\psi}_\tau=-2\frac{\partial\mathcal{F}_q}{\partial Z_-}\ ,\quad \psi_\tau=-2\frac{\partial\mathcal{F}_q}{\partial Z_+}\ . \qquad (2·63)$$

By using these relations, the stationary conditions for NNLO auxiliary fields ($\bar{\psi}_{\tau\tau}$, $\psi_{\tau\tau}$, $\bar{\psi}_{\tau s}$, $\psi_{\tau s}$, $\bar{\psi}_{ss}$, ψ_{ss}) are obtained as

$$\bar{\psi}_{\tau\tau}=2m'_q\bar{\psi}_\tau-\sigma\ ,\quad \psi_{\tau\tau}=2m'_q\psi_\tau-\sigma\ , \qquad (2·64)$$

$$\bar{\psi}_{\tau s} = \bar{\psi}_\tau \psi_\tau \ , \quad \psi_{\tau s} = 2\sigma^2 \ , \quad \bar{\psi}_{ss} = \sigma^2 \ , \quad \psi_{ss} = \sigma^4 \ . \tag{2·65}$$

From Eq. (2·64), we obtain m'_q as a function of $(\sigma, \psi_\tau, \bar{\psi}_\tau)$

$$m'_q = \frac{b'_\sigma\,\sigma + m_0 + 2\beta_{\tau\tau}\sigma}{1 + 2\beta_{\tau\tau}(\psi_\tau + \bar{\psi}_\tau)} \ . \tag{2·66}$$

Now all the stationary values of auxiliary fields other than $(\sigma, \psi_\tau, \bar{\psi}_\tau)$ are obtained as functions of these three fields.

We shall now proceed to erase one more auxiliary field. Three derivatives in Eq. (2·62), $\partial\mathcal{F}_q/\partial m'_q$ and $\partial\mathcal{F}_q/\partial Z_\pm$, are not independent, but are related to the two derivatives, $\partial\mathcal{V}_q/\partial\tilde{m}_q$ and $\partial\mathcal{V}_q/\partial\tilde{\mu}$. The stationary conditions for $\bar{\psi}_\tau$ and ψ_τ in Eq. (2·63) are rewritten in terms of these derivatives as

$$Z_-\bar{\psi}_\tau = \frac{m'_q}{Z_\chi}\frac{\partial\mathcal{V}_q}{\partial\tilde{m}_q} - \frac{\partial\mathcal{V}_q}{\partial\tilde{\mu}} + N_c \tag{2·67}$$

$$Z_+\psi_\tau = \frac{m'_q}{Z_\chi}\frac{\partial\mathcal{V}_q}{\partial\tilde{m}_q} + \frac{\partial\mathcal{V}_q}{\partial\tilde{\mu}} + N_c \ . \tag{2·68}$$

We solve the coupled equations, Eqs. (2·67) and (2·68), for $\partial\mathcal{V}_q/\partial\tilde{m}_q$ and $\partial\mathcal{V}_q/\partial\tilde{\mu}$

$$\frac{\partial\mathcal{V}_q}{\partial\tilde{\mu}} = -\,\omega_\tau(1 - 4m'_q\beta_{\tau\tau}\sigma) \ , \tag{2·69}$$

$$\begin{aligned}\frac{m'_q}{Z_\chi}\frac{\partial\mathcal{V}_q}{\partial\tilde{m}_q} &= \frac{1}{2}(Z_+\psi_\tau + Z_-\bar{\psi}_\tau) - N_c \\ &= \varphi_\tau + \beta'_\tau\bar{\psi}_\tau\psi_\tau + 2\beta_{\tau\tau}m'_q(\bar{\psi}_{\tau\tau}\psi_\tau + \psi_{\tau\tau}\bar{\psi}_\tau) - N_c \ .\end{aligned} \tag{2·70}$$

We have parameterized the auxiliary fields $\bar{\psi}_\tau, \psi_\tau$ as $\bar{\psi}_\tau = \varphi_\tau + \omega_\tau$ and $\psi_\tau = \varphi_\tau - \omega_\tau$. This corresponds to applying the EHS transformation in Eq. (2·25), where we substitute $\phi \to i\omega$. Equation (2·69) implies that ω_τ is related to the quark number density, $\rho_q \equiv -\partial\mathcal{F}_{\text{eff}}/\partial\mu = -\partial\mathcal{V}_q/\partial\tilde{\mu}$. It is also possible to solve the stationary condition for σ in Eq. (2·63) for $\partial\mathcal{V}_q/\partial\tilde{m}_q$.

$$\frac{1}{Z_\chi}\frac{\partial\mathcal{V}_q}{\partial\tilde{m}_q} = -\,\sigma + 2\beta_{\tau\tau}(\bar{\psi}_{\tau\tau}\psi_\tau + \psi_{\tau\tau}\bar{\psi}_\tau) \ , \tag{2·71}$$

Two equations Eqs. (2·70) and (2·71) have to be consistent, then we find the relation between σ, ω_τ and φ_τ

$$\varphi_\tau + \beta'_\tau(\varphi_\tau^2 - \omega_\tau^2) + m'_q\sigma - N_c = 0 \ . \tag{2·72}$$

By substituting Eq. (2·66), we obtain a cubic equation for φ_τ

$$\begin{aligned}&4\beta'_\tau\beta_{\tau\tau}\varphi_\tau^3 + (\beta'_\tau + 4\beta_{\tau\tau} + 2\beta_{\tau s}\sigma^2)\varphi_\tau^2 + (1 - 4N_c\beta_{\tau\tau} - 4\beta'_\tau\beta_{\tau\tau}\omega_\tau^2)\varphi_\tau \\ &\quad -N_c + \sigma[(b_\sigma + 2\beta_{\tau\tau} + 2\beta_s\sigma^2 + 6\beta_{ss}\sigma^4 - 2\beta_{\tau s}\omega_\tau^2)\sigma + m_0] - \beta'_\tau\omega_\tau^2 = 0 \ ,\end{aligned} \tag{2·73}$$

and its solution $\varphi_\tau = \varphi_\tau(\sigma, \omega_\tau)$ is obtained analytically.

We have obtained the final expression of the effective potential as a function of the three auxiliary fields $(\sigma, \varphi_\tau, \omega_\tau)$, temperature T and chemical potential μ

$$\mathcal{F}_{\rm eff} =\mathcal{F}_{\rm eff}^{(X)} + \mathcal{V}_q(\tilde{m}_q; \tilde{\mu}, T) - N_c \log\sqrt{Z_+ Z_-}\ , \tag{2·74}$$

$$\begin{aligned}\mathcal{F}_{\rm eff}^{(X)} =&\frac{1}{2}\tilde{b}_\sigma\,\sigma^2 + \frac{1}{2}\beta_s\sigma^4 + 2\beta_{ss}\sigma^6\\ &+\frac{1}{2}(\beta_\tau + 4\beta_{\tau s}\sigma^2 + 8\beta_{\tau\tau}{m_q'}^2)(\varphi_\tau^2 - \omega_\tau^2) - 4\beta_{\tau\tau}m_q'\varphi_\tau\sigma\ ,\end{aligned} \tag{2·75}$$

$$m_q' =\frac{\tilde{b}_\sigma\sigma + m_0}{1 + 4\beta_{\tau\tau}\varphi_\tau}\ ,\quad \tilde{m}_q = \frac{m_q'}{\sqrt{Z_+ Z_-}}\ , \tag{2·76}$$

$$Z_\pm =1 + (\beta_\tau + 2\beta_{\tau s}\sigma^2 + 8\beta_{\tau\tau}{m_q'}^2)(\varphi_\tau \pm \omega_\tau) - 4\beta_{\tau\tau}m_q'\sigma\ , \tag{2·77}$$

$$\tilde{b}_\sigma =b_\sigma' + 2\beta_{\tau\tau} = b_\sigma + 2\beta_{\tau\tau} + 2\beta_s\sigma^2 + 6\beta_{ss}\sigma^4 + 2\beta_{\tau s}(\varphi_\tau^2 - \omega_\tau^2)\ , \tag{2·78}$$

$$\tilde{\mu} =\mu - \log\sqrt{Z_+/Z_-}\ . \tag{2·79}$$

Since φ_τ is a function of σ and ω_τ whose function form is independent from (T, μ), we cannot regard it as an order parameter. Thus, we have two order parameters in the present treatment of NNLO SC-LQCD, the chiral condensate σ and ω_τ. We can regard ω_τ is a vector potential field for quarks; the chemical potential shift is mainly determined by ω_τ, and ω_τ contributes repulsively to the effective potential in equilibrium. This two order parameter feature may be a natural consequence from the potential term from quarks, $\mathcal{V}_q(\tilde{m}_q; \tilde{\mu}, T)$. There are two independent derivatives, $\partial\mathcal{V}_q/\partial\tilde{m}_q$ and $\partial\mathcal{V}_q/\partial\tilde{\mu}$, which appear in the equilibrium condition, then we have two degrees of freedom.

§3. Chiral Phase Transition in NNLO SC-LQCD

The effective potential derived in the previous section determines the equilibrium (vacuum) and the phase structure of QCD matter. In this section, we investigate the chiral phase transition in the chiral limit $m_0 = 0$ at $N_c = 3$. First, we discuss the effective potential surface and the stationary conditions. Then, critical temperature and chemical potential are investigated. Finally, we discuss the coupling dependence of the critical point.

3.1. *Effective potential surface*

The equilibrium is determined by the stationary condition of $\mathcal{F}_{\rm eff}$ with respect to the auxiliary fields. By substituting φ_τ in Eq. (2·74) with the solution of Eq. (2·73), we obtain the effective potential as a function of σ and ω_τ, $\mathcal{F}_{\rm eff}(\sigma, \omega_\tau) = \mathcal{F}_{\rm eff}(\sigma, \omega_\tau, \varphi_\tau = \varphi_\tau(\sigma, \omega_\tau))$. The remaining stationary conditions are for σ and ω_τ

$$\frac{\partial\mathcal{F}_{\rm eff}}{\partial\sigma} =\frac{\partial\mathcal{F}_{\rm eff}}{\partial\omega_\tau} = 0\ , \tag{3·1}$$

and we have to solve this coupled equation self-consistently. This is equivalent to searching for the saddle point of $\mathcal{F}_{\rm eff}$,[21),34),35)] where $\mathcal{F}_{\rm eff}$ is convex downward and upward in σ and ω_τ directions, $\partial^2\mathcal{F}_{\rm eff}/\partial\sigma^2 > 0$ and $\partial^2\mathcal{F}_{\rm eff}/\partial\omega_\tau^2 < 0$. In Fig. 3, we display $\mathcal{F}_{\rm eff}(\sigma,\omega_\tau)$ at $(T,\mu,\beta)=(0.1,\mu_{c,T=0.1},5.0)$, as an example. The solid curve in Fig. 3 shows the stationary condition for ω_τ, $\omega_\tau=\omega_\tau^{\rm stat.}(\sigma)$, and the filled circles show the equilibrium points. The effective potential as a function of σ for given (T,μ) is defined as $\mathcal{F}_{\rm eff}(\sigma)=\mathcal{F}_{\rm eff}(\sigma,\omega_\tau=\omega_\tau^{\rm stat.}(\sigma))$, whose minimum corresponds to the equilibrium. In the left (right) panel of Fig. 4, we display $\mathcal{F}_{\rm eff}(\sigma)$ on the T-(μ-)axis. The filled circles show the equilibrium points, which are obtained from the stationary condition for σ, Eq. (2·63).

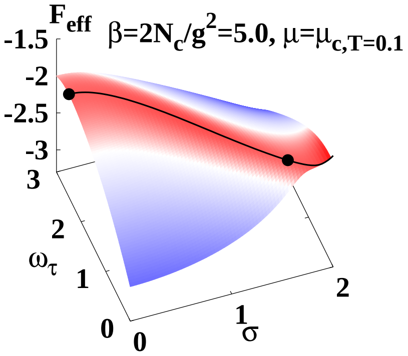

Fig. 3. The effective potential as a function of σ and ω_τ at (T,μ,β)=$(0.1,\mu_c,5.0)$ in the lattice unit. The stationary condition for ω_τ obtained in Eq. (2·69) is satisfied on the solid curve.

In vacuum, the chiral condensate is non-zero, *i.e.* the chiral symmetry is spontaneously broken and the equilibrium is in the NG phase. As temperature increases on the T-axis, the chiral condensate decreases smoothly and become zero at $T=T_{c,\mu=0}$, *i.e.* the chiral phase transition to the Wigner phase takes place. As chemical potential increases on the μ-axis, the chiral condensate changes little and jump to zero at $\mu=\mu_{c,T=0}$. The chiral phase transitions are the second- and the first-order on the T- and the μ-axes, respectively, at $\beta=5.0$. These results are consistent with those in SCL[21), 23)–25), 32)] and NLO[34)] SC-LQCD.

3.2. *Critical temperature and chemical potential*

The second-order phase transition boundary is obtained from the condition of $C_2=0$ where $\mathcal{F}_{\rm eff}(\sigma)=\sum_n C_n\sigma^n/n!$. In order to obtain C_2, we start from the effective potential as a function of σ,φ_τ and ω_τ, $\mathcal{F}_{\rm eff}(\sigma,\omega_\tau,\varphi_\tau)$ in Eq. (2·74). From the stationary conditions, φ_τ and ω_τ are found to be even functions of σ in the chiral limit ($\partial\Phi'/\partial\sigma|_{\sigma=0}=0$, $\Phi'=\varphi_\tau,\omega_\tau$). Because of the stationary condition, the first derivative of $\mathcal{F}_{\rm eff}$ by auxiliary fields are zero ($\partial\mathcal{F}_{\rm eff}/\partial\Phi=0$). By using these properties, C_2 is expressed as,

$$C_2=\left(\frac{\partial}{\partial\sigma}+\sum_{\Phi'=\varphi_\tau,\omega_\tau}\frac{\partial\Phi'}{\partial\sigma}\frac{\partial}{\partial\Phi'}\right)^2\mathcal{F}_{\rm eff}\Bigg|_{\sigma=0}=\frac{\partial^2\mathcal{F}_{\rm eff}}{\partial\sigma^2}\Bigg|_{\sigma=0} \qquad (3·2)$$

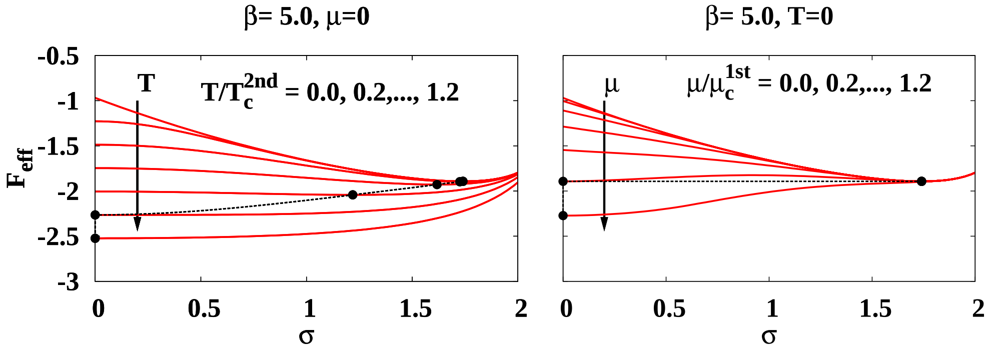

Fig. 4. The effective potential in the lattice unit is illustrated as a function of the chiral condensate σ on the T-axis (left) and the μ-axis (right) for $\beta = 5.0$. The filled circles show the equilibrium points. In the left (right) panel, the effective potential decreases for increasing $T(\mu)$.

$$=C_2^{(X)} + C_2^{(\mathcal{V}_q)} - \frac{N_c}{2}\left[\frac{C_2^{(Z_+)}}{Z_+} + \frac{C_2^{(Z_-)}}{Z_-}\right] , \tag{3·3}$$

where,

$$C_2^{(X)} = \frac{\partial^2 \mathcal{F}_{\rm eff}^{(X)}}{\partial \sigma^2} = \tilde{b}_\sigma + \left(4\beta_{\tau s} + 8\beta_{\tau\tau} C_{m_q'}^2\right)(\varphi_\tau^2 - \omega_\tau^2) - 8\beta_{\tau\tau}\varphi_\tau C_{m_q'} , \tag{3·4}$$

$$C_2^{(\mathcal{V}_q)} = \frac{\partial^2 \mathcal{V}_q}{\partial \sigma^2} = \frac{\rho_q}{2}\left[\frac{C_2^{(Z_+)}}{Z_+} - \frac{C_2^{(Z_-)}}{Z_-}\right] - \frac{N_c(N_c+1)(N_c+2)}{3T(2\cosh(N_c\tilde{\mu}/T) + N_c + 1)} \cdot \left(\frac{C_{m_q'}}{Z_\chi}\right)^2 , \tag{3·5}$$

$$C_2^{(Z_\pm)} = \frac{\partial^2 Z_\pm}{\partial \sigma^2} = \left(4\beta_{\tau s} + 16\beta_{\tau\tau} C_{m_q'}^2\right)(\varphi_\tau \pm \omega_\tau) - 8\beta_{\tau\tau} C_{m_q'} , \tag{3·6}$$

$$C_{m_q'} = \frac{m_q'}{\sigma} = \frac{\tilde{b}_\sigma}{1 + 4\beta_{\tau\tau}\varphi_\tau} . \tag{3·7}$$

In Eqs.(3·3)–(3·7), the right hand sides have to be evaluated in the conditions $\sigma = 0$ and $\rho_q = -\partial\mathcal{V}_q/\partial\tilde{\mu}$.

The second order critical temperature at $\mu = 0$ is obtained from the condition $C_2 = 0$ at $\mu = 0$ as

$$T_{c,\mu=0} = T_c^{(\rm SCL)} \cdot \frac{C_{m_q'}^2}{b_\sigma Z_\chi^2}\left(C_2^{(X)} - \frac{N_c C_2^{(Z_+)}}{Z_+}\right)^{-1} , \tag{3·8}$$

where $T_c^{(\rm SCL)} = d(N_c+1)(N_c+2)/[6(N_c+3)]$ denotes the critical temperature at $\mu = 0$ in the strong coupling limit. Note that at $\mu = 0$, ω_τ becomes zero (i.e. $\tilde{\mu} = 0$). Therefore, the coefficients in $T_{c,\mu=0}$ are the value at $\omega_\tau = 0$, and then we find $Z_+ = Z_-$ ($C_2^{Z_+} = C_2^{Z_-}$). $T_{c,\mu=0}$ decreases as β increases because of finite coupling effect.

In Fig. 5, we compare the critical temperature in NLO and NNLO. In both NLO and NNLO, $T_{c,\mu=0}$ decreases as β increases, and $T_{c,\mu=0}$ in NLO and NNLO exhibit

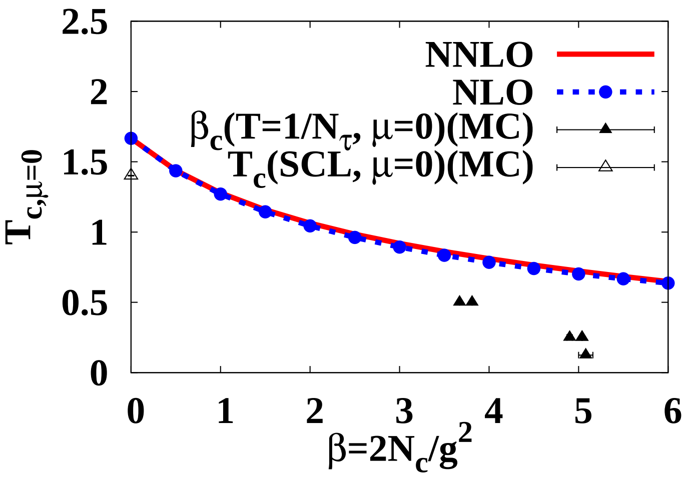

Fig. 5. The β dependences of the critical temperature at $\mu = 0$ ($T_{c,\mu=0}$) in the lattice unit. We compare the NLO (the dashed line with circles) and NNLO (the solid line) results. The triangles represent the results of the critical temperature ($T_{c,\mu=0}$, open triangle) and the critical coupling (β_c, filled triangles) obtained in Monte-Carlo simulations with one species of unrooted staggered fermion: From the left, $T_{c,\mu=0}$ in the SCL with MDP simulations,[32] β_c at $(N_\tau, m_0) = (2, 0.025)$,[38] $(2, 0.05)$,,[38] $(4, 0.0)$,[39] $(4, 0.05)$,[36),37] and $(8, 0.0)$.[40]

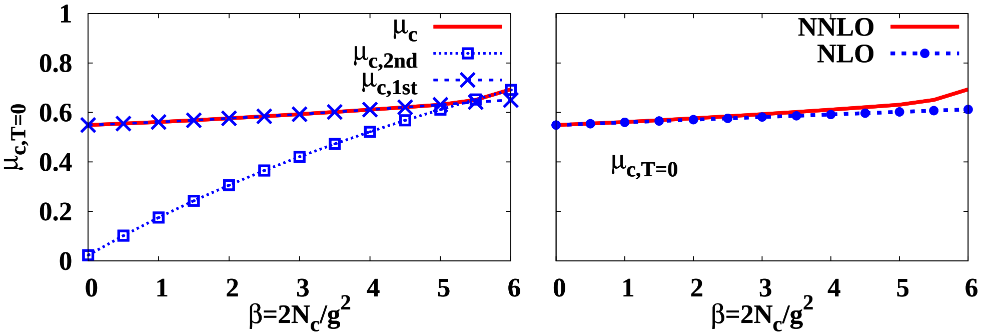

Fig. 6. The β dependences of the critical chemical potential at $T = 0$ ($\mu_{c,T=0}$) in the lattice unit. In the left panel, we show NNLO results for the critical chemical potential (the solid line), the first-order critical chemical potential (the dashed line with crosses) and the second-order critical chemical potential (the dotted line with squares). In the right panel, we compare the NLO (the dashed line with circles) and NNLO (the solid line) results.

almost the same values. We also show the MC results with one species of unrooted staggered fermion on the critical coupling (β_c) for given $N_\tau = 1/T = 2, 4$ and 8 at $\mu = 0$ (filled triangles) and the critical temperature in SCL: From the left, we show $T_{c,\mu=0}$ in the SCL with monomer-dimer-polymer (MDP) simulations,[32] β_c at $N_\tau = 2$ (the quark mass $m_0 = 0.025$),[38] $N_\tau = 2$ ($m_0 = 0.05$),[38] $8^3 \times 4$ lattice (with a chiral extrapolation),[39] $8^3 \times 4$ lattice ($m_0 = 0.05$),[36] $6^3 \times 4$ lattice ($m_0 = 0.05$),[37] and

$N_\tau = 8$ (with a chiral extrapolation).[40] The reduction of $T_{c,\mu=0}$ is not enough to explain the MC results. In this formulation, we do not consider the deconfinement phase transition and the quarks are confined. $T_{c,\mu=0}$ could decrease than NNLO results from the effects of the Polyakov loop which is an order parameter of the deconfinement phase transition.[45] In NNLO, the phase transition at $\mu = 0$ stays to be the second order in the region $\beta \leq 6$. This point differs from the numerical simulation results, where the phase transition at $\mu = 0$ is shown to be the first order in the continuum region.[36] The relation with the critical point position will be discussed in the next subsection.

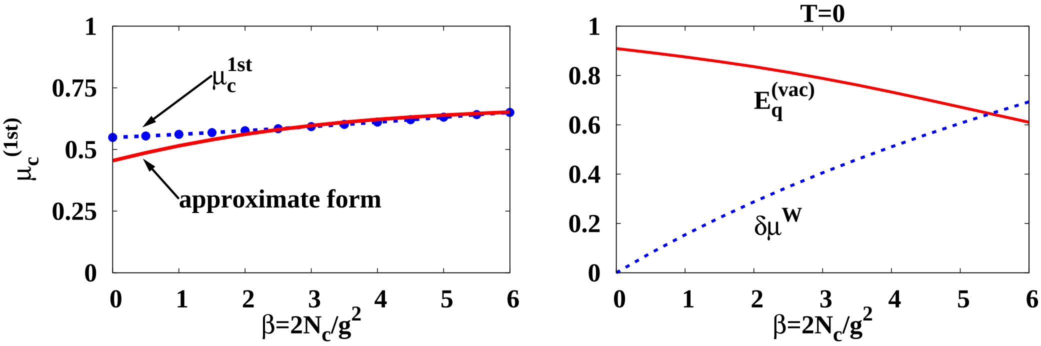

Fig. 7. In the left panel, we show the critical chemical potential at $T = 0$ ($\mu_c^{(1st)}$, the dashed line with circles). The result obtained by "approximate expression", $(E_q^{(vac)} + \delta\mu^W)/2$, is also shown for a comparison (the solid line). In the right panel, we compare at $T = 0$ a mass modification $E_q^{(vac)}$ (the upper solid line) with a chemical potential modification $\delta\mu^W$ (the lower dashed line) as a function of β. In both panels, we use the lattice unit.

In Fig. 6, the phase transition on μ-axis is numerically found to be the first-order for $\beta \lesssim 5.5$. We find that $\mu_{c,T=0}^{(1st)}$ is not largely affected by finite coupling effects. This is understood as follows. Taking the limit $T \to 0$ in Eq. (2·52), one can easily derive that the quark free energy reduces to

$$\mathcal{V}_q = \left\{ \begin{array}{ll} -N_c E_q & (E_q \geq \tilde{\mu}) \\ -N_c \tilde{\mu} & (E_q \leq \tilde{\mu}) \end{array} \right. . \tag{3·9}$$

As explained after Eq. (2·54), E_q represents the quark excitation energy. In this formulation, we do not consider the deconfinement phase transition and the quarks are confined. Then, the one and two quark excitation contribution disappears after temporal link (U_0) integration. As a result, the factor N_c accompanies E_q in Eq. (3·9). This means that the contribution from three co-moving quarks appear as a baryon in the effective potential at low T.

At $\mu = \mu_{c,T=0}^{(\mathrm{1st})}$, effective potentials at two local minima are the same, then the following relation holds

$$\begin{aligned} &-\frac{1}{2}N_c E_q^{\mathrm{NG}} + \left(-\frac{1}{2}N_c E_q^{\mathrm{NG}} + \mathcal{F}_{\mathrm{eff}}^{(X),\mathrm{NG}} - N_c \log Z_\chi^{\mathrm{NG}}\right) \\ &\quad = -N_c\mu + \frac{1}{2}N_c\delta\mu^{\mathrm{W}} + \left(\frac{1}{2}N_c\delta\mu^{\mathrm{W}} + \mathcal{F}_{\mathrm{eff}}^{(X),\mathrm{W}} - N_c \log Z_\chi^{\mathrm{W}}\right) , \end{aligned} \tag{3·10}$$

where the lhs and rhs show the effective potentials in the Nambu-Goldstone (NG) and the Wigner phases, respectively. We numerically find that the lhs and rhs in the brackets have almost the same values. Then, the above relation is approximately represented as

$$-\frac{1}{2}N_c E_q^{\mathrm{NG}} \simeq -N_c\mu + \frac{1}{2}N_c\delta\mu^{\mathrm{W}} \ , \tag{3·11}$$

These approximate expressions are explained based on the two-body interaction dominance, where the total potential energy amounts to be half of the single particle potential. This relation is exact when the effective potential is a quadratic function of σ or ω_τ. In the NG phase, the quark number density is very small at $T = 0$, then the main contribution to the potential energy comes from σ. In the Wigner phase, the chiral symmetry is restored, then the effective potential becomes a function of ω_τ. Since there are contributions from other auxiliary fields and the quark free energy is not a linear function of σ or ω_τ, the above relation is an approximate one. In the NG phase at $T = 0$, the quark number density is almost zero, and the quark excitation energy is almost the same as that in vacuum, $E_q^{\mathrm{NG}}(\mu > 0) \simeq E_q^{\mathrm{NG}}(\mu = 0) \equiv E_q^{(\mathrm{vac})}$. In addition, we obtain $\omega_\tau = \rho_q \simeq N_c$ in the Wigner phase at $T = 0$. By using these facts, the Eq. (3·11) reduces to,

$$\mu_{c,T=0}^{(\mathrm{1st,App.})} = \frac{1}{2}\left[E_q^{(\mathrm{vac})} + \delta\mu^{\mathrm{W}}\right] \ , \tag{3·12}$$

$$\delta\mu^{\mathrm{W}} = \delta\mu(\sigma = 0, \omega_\tau = N_c) \ . \tag{3·13}$$

In the left panel of Fig. 7, we compare the first order critical chemical potential with its approximate expression in Eq. (3·12). For $\beta \gtrsim 3$, $\mu_{c,T=0}^{(\mathrm{1st,App.})}$ can roughly explain $\mu_{c,T=0}^{(\mathrm{1st})}$.

In the right panel of Fig. 7, we show the β dependence of E_q and $\delta\mu$. With increasing β, E_q becomes smaller but $\delta\mu^{\mathrm{W}}$ goes to a larger value. The sum of them appearing in Eq. (3·12) slightly increases and is not very sensitive to β. Thus, the quark mass (or excitation energy) and chemical potential suppressions which come from the finite β effects cancel each other out, and we observe a small modification of the critical chemical potential.

3.3. *Critical point evolution*

In Fig. 8, we show the critical point (CP) evolution with β in NNLO (the solid line with circles) and NLO (the dashed line with circles). We find that the CP stays to be the tri-critical point (TCP) in NNLO. This point is different from NLO results, where TCP starts to deviate from the second order boundary at $\beta \simeq 4.5$ and becomes critical end point (CEP) for larger β.[34),35)] While the temperature of CP decreases in both NNLO and NLO, we find different behavior in the chemical potential of CP, μ_{CP}. In NNLO (NLO), CP moves in the smaller (larger) μ direction with increasing β in the range $\beta \gtrsim 3$. The behavior in NNLO is favorable, since the phase transition with one species of unrooted staggered fermion at $\mu = 0$ is numerically shown to be the first order in the continuum region.[36)]

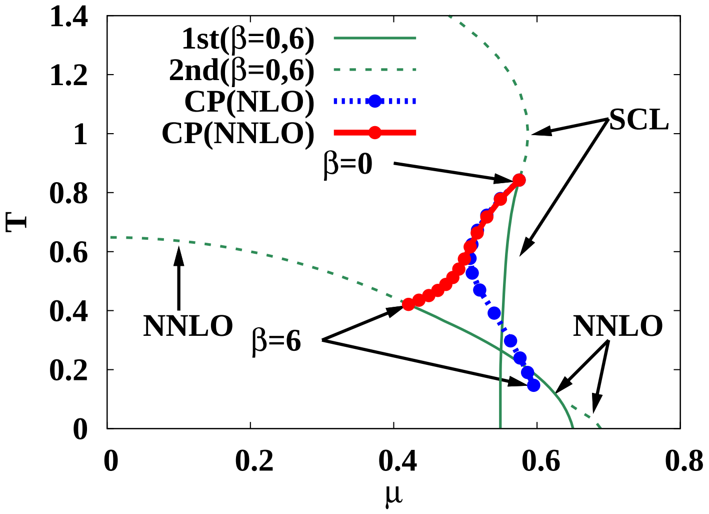

Fig. 8. The critical point (CP) flow resulting from increasing β in $T-\mu$ plane in the lattice unit. The solid and the dotted lines represent trajectories of NNLO and NLO cases, respectively. We also show the first and second-order phase transition boundaries obtained in cases of SCL and NNLO at $\beta=6$.

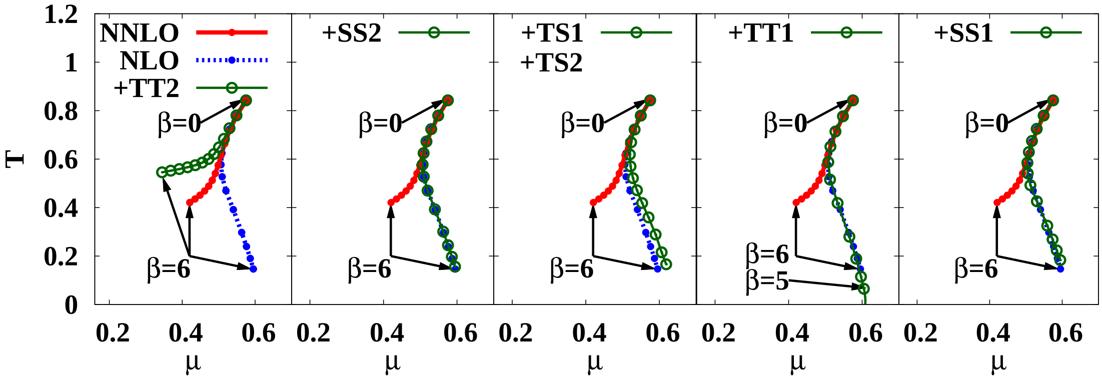

Fig. 9. The critical point flow with increasing β in several truncation schemes in the lattice unit. From the left panel, a part of NNLO effects, NNLO-TT2, NNLO-SS2, NNLO-TS12, NNLO-TT1 or NNLO-SS1 is taken into account. We compare them with NLO (the dotted line with circles) and full NNLO (the solid line with circles) results.

The above behavior of $\mu_{\rm CP}$ is caused by the two temporal plaquette diagram, NNLO-TT2. In NNLO, the diagrams with connected two plaquette configurations shown in Fig. 2 contribute to the effective action. In Fig. 9, we show the effects of each NNLO diagram on the CP evolution. From the left, we consider the effective action terms only from the NNLO-TT2, NNLO-SS2, NNLO-TS1+NNLO-TS2, NNLO-TT1 or NNLO-SS1 diagram. We find only the NNLO-TT2 shifts CP in the lower μ direction. The other NNLO diagrams do not modify the direction of CP evolution with β. The temporal hopping of quarks, that is the thermal effect of quarks, seems

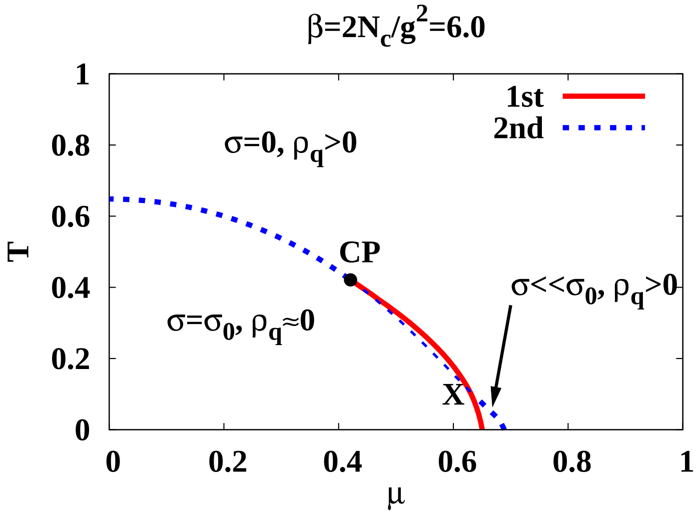

Fig. 10. The NNLO phase diagram at $\beta = 6.0$ in the lattice unit. The solid and thick dashed lines represent the first- and second-order phase transition boundaries, respectively. The filled circle represents the tri-critical point. On the (thick and thin) dashed line, $C_2 = 0$ is satisfied, where C_2 is the curvature of the effective potential in Eq. (3·2). Note that there is no phase transition on the thin dashed line between CP and X. By contrast, in the region where T is lower than that of X, two sequential phase transitions occur as μ becomes large.

to be essential for the suppression of μ_{CP} at larger β.

In Fig. 10, we display the phase diagram at $\beta = 6.0$. The NG phase ($\sigma \neq 0$) appears in low T and low μ region, and the Wigner phase ($\sigma = 0$) appears at high T or high μ. We find that the second-order phase boundary obtained by $C_2 = 0$ exceeds the first-order one in low T region. Between those boundaries, we observe an interesting matter state where the effective chemical potential $\tilde{\mu}$ is adjusted to be around the quark excitation energy E_q. In other words, the chiral symmetry is partially restored to satisfy the balance relation $\tilde{\mu} \simeq E_q$, which leads to an intermediate value of the quark number density ρ_q. In this partially chiral restored (PCR) matter, N_c quarks are co-moving and they have a smaller constituent quark mass; the former shows the confined nature and the latter is due to the partial chiral restoration. When the PCR matter appears, two sequential phase transitions take place as μ becomes large with the balance relations $\tilde{\mu} \simeq E_q(\sim \tilde{m}_q)$. This phase transition pattern is consistent with the implication from the large N_c argument, *i.e.* the quarkyonic transition[46] as discussed in our previous works.[34],[35] In order to clarify the relation of the PCR phase and the quarkyonic matter, it would be necessary to take account of the deconfinement transition, which will be reported elsewhere.[45]

While it is still uncertain that the PCR matter realizes in the continuum limit, we emphasize that this third phase (besides NG and Wigner phases) has been commonly observed in the T-μ-β space in the NLO [34],[35] and NNLO SC-LQCD via the self-consistent treatment of the vector potential ω_τ. Compared to NLO results,[34],[35] PCR phase appears in the lower T region in the present work. NNLO-TT1 and NNLO-TT2 are found to be responsible for such a tendency.

§4. Summary

In this paper, we have derived an analytic expression of the effective potential at finite temperature and density including the next-to-next-to-leading (NNLO) effects in the strong coupling expansion of the lattice QCD, and investigated NNLO effects on the chiral phase transition and its phase diagram. We adopt one species of unrooted staggered fermion corresponding to $N_f = 4$ in the continuum region. Effective action terms have been systematically evaluated based on the strong coupling expansion. We have concentrated on the leading order of the $1/d$ expansion, then the NNLO effective action terms are generated from six types of two plaquette configurations. We have applied the extended Hubbard-Stratonovich transformation[34),35)] in order to bosonize fermion interaction terms. We encounter those terms containing the interaction between the next-to-nearest neighbor sites $(x, x+2\hat{0})$ arising from $1/g^4$ terms of the effective action. These effects can be evaluated by introducing the gluonic dressed fermion, which leads to modifications of temporal quark hopping and mass terms. We have obtained the effective potential as a function of temperature (T), chemical potential (μ) and the two order parameters: the chiral condensate (σ) and the vector potential (ω_τ). The equilibrium is determined from the stationary condition of the effective potential with respect to the auxiliary fields. NLO and NNLO effects result in modification of the wave function renormalization factor, quark mass and chemical potential. The effective chemical potential reflects the repulsive contribution of the vector potential.

We have found that the critical temperature at $\mu = 0$ ($T_{c,\mu=0}$) is largely suppressed with increasing β. In comparison, the chemical potential at $T = 0$ ($\mu_{c,T=0}$) is a slightly increasing function of β. These behaviors of the critical temperature and chemical potential in NNLO are consistent with those in NLO in the region $\beta \leq 6.0$. The behaviors $\mu_{c,T=0}$ and $T_{c,\mu=0}$ are understood from the quark mass reduction, and its cancellation with quark chemical potential reduction, respectively.

We have found that the critical point (CP) moves to lower T direction with increasing β in both NLO and NNLO. In NNLO, the chemical potential of the critical point decreases with increasing β. This shift is opposite to the NLO case with $\beta \gtrsim 3.0$.[34),35)] Thus, the critical point (CP) flow with increasing β is sensitive to $1/g^4$ effects, and the first-order transition tends to dominate the phase boundary as β is increased in NNLO. The NNLO CP flow would be favorable because the phase transition at $\mu = 0$ is shown to be the first order for the unrooted staggered fermion in the continuum region.[36)] We have found that the next-to-nearest neighbor interaction makes the CP flow go to a lower μ direction.

In low T and high μ region, we have found the partially chiral restored (PCR) phase where effective chemical potential is always adjusted to be around the quark excitation energy. The PCR matter is obtained also in NLO as long as the two order parameter (σ and ω_τ) are introduced. The appearance of PCR matter would be a common consequence in NLO and NNLO SC-LQCD with finite coupling effects.

There are several points to be studied in future. Firstly, the Polyakov loop can be constructed by using two plaquettes in the NNLO SC-LQCD with $N_\tau = 2$. This effect has not been considered in the present analyses, and quarks are confined. It is interesting to investigate the deconfinement transition in addition to the chiral phase transition by considering the Polyakov loop effects. Secondly, we should study the higher order of the $1/d$ expansion, which contains the spatial baryon hoppings and could play an essential role at finite density on the lattice.

Acknowledgments

We would like to thank Professor Philippe de Forcrand for useful discussions. This work was supported in part by the Grant-in-Aid for Scientific Research by MEXT and JSPS (nos. 17070002 and 19540252), the Yukawa International Program for Quark-hadron Sciences (YIPQS), and by the Grant-in-Aid for the global COE program 'The Next Generation of Physics, Spun from Universality and Emergence' from MEXT.

References

1) For a recent review, see B. Müller and J. L. Nagle, Ann. Rev. Nucl. Part. Sci. **56**, (2006) 93.
2) For a recent review, see S. Muroya, A. Nakamura, C. Nonaka and T. Takaishi, Prog. Theor. Phys. **110** (2003), 615;
F. Karsch, Prog. Theor. Phys. Suppl. **153** (2004), 106.
3) K. G. Wilson, Phys. Rev. D **10** (1974), 2445.
4) M. Creutz, Phys. Rev. D **21** (1980), 2308;
M. Creutz and K. J. M. Moriarty, Phys. Rev. D **26** (1982), 2166.
5) G. Münster, Nucl. Phys. B **180** (1981), 23.
6) N. Kawamoto and J. Smit, Nucl. Phys. B **192** (1981), 100.
7) J. Hoek, N. Kawamoto and J. Smit, Nucl. Phys. B **199** (1982), 495.
8) J. Smit, Nucl. Phys. B **175** (1980), 307.
9) H. Kluberg-Stern, A. Morel, O. Napoly and B. Petersson, Nucl. Phys. B **190** (1981), 504.
10) D. B. Kaplan, Phys. Lett. B **288** (1992), 342.
11) H. Neuberger, Phys. Lett. B **427** (1998), 353.
12) R. C. Brower and B. Svetitsky, Phys. Rev. D **61** (2000), 114511.
13) L. Levkova and R. Mawhinney, Nucl. Phys. Proc. Suppl. **140** (2005), 695.
14) I. Ichinose and K. Nagao, Nucl. Phys. B **577** (2000), 279;
Nucl. Phys. B **596** (2001), 231.
15) P. Ye, X. L. Yu, Y. Guan and X. Q. Luo, Mod. Phys. Lett. A **22** (2007), 547;
X. L. Yu and X. Q. Luo, Mod. Phys. Lett. A **22** (2007), 537.
16) P. H. Damgaard, N. Kawamoto and K. Shigemoto, Phys. Rev. Lett. **53** (1984), 2211;
Nucl. Phys. B **264** (1986), 1.
17) P. H. Damgaard, D. Hochberg and N. Kawamoto, Phys. Lett. B **158** (1985), 239.
18) G. Faldt and B. Petersson, Nucl. Phys. B **265** (1986), 197.
19) E. M. Ilgenfritz and J. Kripfganz, Z. Phys. C **29** (1985), 79.
20) A. Gocksch and M. Ogilvie, Phys. Rev. D **31** (1985), 877.
21) N. Bilic, K. Demeterfi and B. Petersson, Nucl. Phys. B **377** (1992), 651;
N. Bilic and J. Cleymans, Phys. Lett. B **355** (1995), 266.
22) N. Bilic, F. Karsch and K. Redlich, Phys. Rev. D **45** (1992), 3228.
23) Y. Nishida, K. Fukushima and T. Hatsuda, Phys. Rept. **398** (2004), 281.
24) K. Fukushima, Prog. Theor. Phys. Suppl. **153** (2004), 204.
25) Y. Nishida, Phys. Rev. D **69** (2004), 094501.
26) V. Azcoiti, G. Di Carlo, A. Galante and V. Laliena, J. High Energy Phys. **09** (2003), 014.
27) N. Kawamoto, K. Miura, A. Ohnishi and T. Ohnuma, Phys. Rev. D **75** (2007), 014502.

28) K. Fukushima, Phys. Lett. B **553** (2003), 38; K. Fukushima, Phys. Rev. D **68** (2003), 045004.
29) N. Kawamoto and K. Shigemoto, Phys. Lett. B **114** (1982), 42;
Nucl. Phys. B **237** (1984), 128.
30) H. Kluberg-Stern, A. Morel and B. Petersson, Nucl. Phys. B **215** (1983), 527.
31) T. Jolicoeur, H. Kluberg-Stern, M. Lev, A. Morel and B. Petersson, Nucl. Phys. B **235** (1984), 455.
32) P. de Forcrand and M. Fromm, arXiv:0907.1915 [hep-lat].
33) F. Karsch and K. H. Mütter, Nucl. Phys. B **313** (1989), 541.
34) K. Miura, T. Z. Nakano, A. Ohnishi and N. Kawamoto, Phys. Rev. D **80** (2009), 074034.
35) K. Miura, T. Z Nakano and A. Ohnishi, Prog. Theor. Phys. **122** (2009), 1045.
36) M. D'Elia and M. P. Lombardo, Phys. Rev. D **67** (2003), 014505.
37) Z. Fodor and S. D. Katz, Phys. Lett. B **534** (2002), 87.
38) P. de Forcrand (private communication).
39) S. A. Gottlieb, W. Liu, D. Toussaint, R. L. Renken and R. L. Sugar, Phys. Rev. D **35** (1987), 3972.
40) R. V. Gavai *et al.* [MT(c) Collaboration], Phys. Lett. B **241** (1990), 567.
41) L. Susskind, Phys. Rev. D **16** (1977), 3031.
42) H. S. Sharatchandra, H. J. Thun and P. Weisz, Nucl. Phys. B **192** (1981), 205.
43) P. Hasenfratz and F. Karsch, Phys. Lett. B **125** (1983), 308.
44) For example, R. Kubo, J. Phys. Soc. Jap. **17** (1962), 1100.
45) T. Z. Nakano, K. Miura and A.Ohnishi, in preparation.
46) L. McLerran and R. D. Pisarski, Nucl. Phys. A **796** (2007), 83;
Y. Hidaka, L. D. McLerran and R. D. Pisarski, Nucl. Phys. A **808** (2008), 117.
47) R. D. Pisarski and F. Wilczek, Phys. Rev. D **29** (1984), 338.
48) A. S. Kronfeld, PoS **LAT2007** (2007), 016.
49) S. R. Sharpe, PoS **LAT2006** (2006), 022.
50) M. Creutz, Phys. Lett. B **649** (2007), 230.
51) E. Seiler, Lect. Notes Phys. **159** (1982), 1; K. Osterwalder and E. Seiler, Annals Phys. **110** (1978), 440.
52) G. Boyd, J. Fingberg, F. Karsch, L. Karkkainen and B. Petersson, Nucl. Phys. B **376** (1992), 199.
53) K. Fukushima, Phys. Lett. B **591** (2004), 277 .
54) C. Ratti, M. A. Thaler and W. Weise, Phys. Rev. D **73** (2006), 014019 .
55) K. Kashiwa, H. Kouno, M. Matsuzaki and M. Yahiro, Phys. Lett. B **662** (2008), 26;
Y. Sakai, K. Kashiwa, H. Kouno and M. Yahiro, Phys. Rev. D **77** (2008), 051901.